INSTITUTE
FOR
AEROSPACE STUDIES

UNIVERSITY OF TORONTO

RESEARCH ON AN AERODYNAMIC PARTICLE SEPARATOR

(THE EPS)

by

B. Etkin

July 1986

UTIAS Report No. 316
CN ISSN 0082-5255

RESEARCH ON AN AERODYNAMIC PARTICLE SEPARATOR

(THE EPS)

by

Bernard Etkin

Submitted May 1986

July 1986

UTIAS Report No. 316
CN ISSN 0082-5255

Acknowledgement

The research reported in this paper was supported by the Natural Science and Engineering Research Council of Canada through operating grant No. A0339, and PRAI grant No. P8212 with the cooperation of W. S. Tyler of St. Catharines, Ontario. Most of the design, analysis, and experimental work reported was carried out under the direction and supervision of the author by researchers Norbert Fan, Donald McTavish and Kenny Eom.

Abstract

This report presents an account of the research work carried out in support of the development of a new particle separator. The EPS, as it is designated, produces multiple fractions simultaneously at a high throughput rate. The cut sizes are roughly in the range 10 to 200 μm. The principle is that particles dissimilar with respect to any of size, density, or shape will follow different and distinct trajectories when injected into a uniform laminar flow of air. The main features of the design are:

(1) particles are conveyed pneumatically at high speed into the separation zone;

*(2) they are separated from the feed air at the entrance to the separation zone by means of the Coanda Effect;

(3) the air flow in the separation zone is uniform and laminar, the rms turbulence level being less than 1%; air speed in the separation zone is of the same order as the particle speed;

(4) the particles are subjected to large forces, both aerodynamic and mechanical, at several points on their path from the feed hopper to the separation zone, thus promoting dispersion.

The report contains the theoretical analyses and experimental measurements made to verify the design concepts. A detailed model of the flow field permits the calculation of particle trajectories, and hence the prediction of coarse grade efficiency and sharpness of cut d_{25}/d_{75}. The measurements made with glass spheres and other irregular particles (e.g., carbon, cement) provide a general verification of the analytical results.

Sharpness of cut values better than 0.8 are achieved down to cut points of about 10 μm. Maximum throughput rates are not yet known, but separations have been made at 480 kg/hr in a separation zone 100 mm wide. Scale-up to larger capacity is straightforward.

---

*U.S. Patent allowed and to be issued.

Contents

Notation

$C_D = D/\frac{1}{2}\rho V_r^2 S$	Drag coefficient
d	Particle diameter
d_{25}, d_{50}, d_{75}	Particle diameters that have {25, 50, 75}% chance of reporting to the coarse stream
D	Drag of particle
m	Mass of particle
r, r_i	See Fig. 3
$Re = V_r d\rho/\mu$	Reynolds number
$S = \pi d^2/4$	Reference area for particle
s.g.	Specific gravity of particle
t'	Thickness of Coanda zone (Fig. 3)
t	Thickness of entry slit (Fig. 3)
u_m	See Fig. 4
U	speed of main separation air
$\underline{V}_a(u_a, v_a)$	Velocity of the air
V_F	Speed of feeder jet at the entry slit
$\underline{V}_p$	Velocity of particle
V_{p_o}	Initial speed of particle
$\bar{V}_p$	Mean particle speed at entry slit
$\underline{V}_r = \underline{V}_p - \underline{V}_a$	Velocity of particle relative to local airstream
$\beta = d_{25}/d_{75}$	Sharpness of cut parameter
λ	Empirical parameter
ρ	Density of air (1.2 kg/m^3)
σ	Standard deviation of particle speed at entry to the separator
$\sigma = \sigma/\bar{V}_p$	Normalized standard deviation

μ	Viscosity of air ($1.8\ kgm^{-1}\ sec^{-1}$)
$\xi = r - r_i$	See Fig. 3
ξ_m	See Fig. 4
$\xi_{m/2}$	A parameter of the Coanda flow field
$\eta(d)$	Probability that a particle of size d will be collected in the coarse stream (coarse grade efficiency)

I. INTRODUCTION

Previous research at UTIAS led to the development of the TERVEL separator, a particle separator (air classifier) that operates on differences in the terminal velocity of the particles that pass through it [1, 2]. In that separator the particles are fed in vertically by gravity at low velocity, and are carried horizontally by an air stream through a distance that is proportional to the time of fall. The trajectories terminate in some form of collector. This device exists in two embodiments[1] — the model L for laboratory processing of small samples, and the model P for industrial processing of large tonnages. The TERVEL separator was developed with special attention to its aerodynamic characteristics, so that the separation zone is a flow-field of high uniformity, and low turbulence. This device yields multiple fractions of the product (the number is arbitrary and may be large if desired) and has achieved sharpness of cut values $\beta = d_{25}/d_{75}$ of 0.9. This represents very high performance for an air classifier.

The TERVEL separator has two limitations that restrict its effective application to materials generally larger than about 50 μm. The first of these limitations is that finer materials frequently display agglomeration that causes the particles to pass through the separation zone in clumps instead of as individuals. These clumps of course behave as single large particles and hence report to the wrong output collector. This limitation is operative for both Models L and P. The second limitation is that the presence of mutual aerodynamic interference of the particles in their descent through the separation zone sets an upper limit to the mass flow that can be accommodated without degradation of the performance. For small monosized particles this mass-flow limit varies approximately as the cube of the particle diameter, and hence the capacity of the model P diminishes rapidly with decreasing particle size. This feature does not affect the model L, since laboratory samples are in any case processed in a minute or so.

The basic reason for the second limitation, on throughput, is that the air speed in the separation zone must be kept more-or-less proportional to the terminal velocity of the particles, otherwise the particle trajectories become impractically slanted. Hence the air speed becomes very small (< 0.1 m/s) for particles smaller than about 40 μm. This is an inherent property of all gravity-fed "cross-flow" air classifiers (in which particle trajectories cross the streamlines of the flow). Clearly, in order to remove this limitation, it is necessary to design a system in which the air speed is high, and hence in which the particles are injected into the airstream at a correspondingly high speed. This precludes entirely the use of gravity as the particle-propelling force in any practical scheme. As we shall see in the following, the high-speed configuration that we developed is not a simple cross-flow separator. Configurations of this general class have previously been investigated extensively by Rumpf and Leschonski [3, 4, 5].

The central features of the design studied in this report are:

1. the particles are conveyed pneumatically into the separation zone,

---

[1] Marketed by the W. S. Tyler Co., Mentor, Ohio, and St. Catharines, Ontario.

2. they are separated from the feed air at the entrance to the separation zone by means of the "Coanda Effect" [6],[2]

3. the air flow in the separation zone is uniform and laminar by virtue of both upstream and downstream features of the ducting, and by virtue of the diversion of the feed stream by the Coanda Effect,

4. the particles are subjected to large forces, both aerodynamic and mechanical, thus promoting dispersion of agglomerations.

The design that has evolved from this research is designated the EPS.[3] In the following sections we describe the EPS and the theoretical and experimental results of the research.

II. DESCRIPTION OF THE EPS

The general arrangement of the laboratory apparatus is as sketched in Fig. 1. The solid particulates to be processed are introduced into the hopper, from which they are passed by a rotary air-locked feeder into the feed-air channel. They are then blown through this channel and injected into the separation zone at high speed.

Air for the separation zone is supplied by a second system, comprising a blower and ducting. This is designed to generate a uniform laminar flow within the separation zone. To this end the ducting consists of a diffuser that provides a transition between the blower discharge and a parallel rectangular section containing wire screens. This is followed by a two-dimensional contraction, designed by the hodograph method [7] to yield the desired uniformity of velocity at its discharge. The separation air velocity used is generally in the same range as the feed air. Both air supplies are controllable to permit continuous adjustment of the two flows. For low solid feed rates, a vacuum cleaner was used to supply the feed air, with RPM controlled by a variable transformer. For higher feed rates we used the laboratory compressed air supply, metered through a control valve. In the latter case we achieved constant air mass-flow against a variable load by using choked flow at the valve. The airspeed in the separation zone was controlled by driving the blower with a variable-speed motor. The solids flow rate was controlled by running the rotary feeder with a variable-speed motor.

Figure 2 shows one of the configurations we have tested for the separation zone, and an example of some computed trajectories for $U = V_f = 10$ m/s, and particles of s.g. 2.0. The feed-air carrying the particles enters at C through a thin slit. Adjacent to the slit, on the downstream side, is a circular quadrant, which forms the attachment surface for the feed jet. The Coanda effect ensures that the feed-air jet adheres to this curved surface provided that the ratio r_i/t (see Fig. 3) is large enough and that the solids feed rate does not exceed some upper limit. Thus the air carrying the particles is rapidly turned through 90° into the downstream direction. The entrained particles, at any rate those larger than some minimum size, are unable to

---

[2] There is a large literature on the Coanda effect. Reference [6] contains the principal data we used to model our flow field.

[3] Patent pending.

follow the air, and are flung out, so to speak, by centrifugal force. The feed air, being confined to a narrow layer adjacent to the roof of the chamber, does not interfere significantly with the separation air, which thus retains its desirable features of uniformity and laminarity — except of course to the extent that these are disturbed by the particles themselves.

On their way from the hopper to the separator, the particles are subjected to large aerodynamic forces at A and C (Fig. 1) and to a large mechanical force at the bend B. The role of the latter in dispersing agglomerations is self-evident. The utility of large aerodynamic forces can be inferred from the work of Suganuma et al [9]. They showed that passing agglomerations at high speed through narrow pipes, orifices or ejectors is effective in promoting dispersion. The underlying cause in each case is the application of a large aerodynamic force to the clump, which has the effect of pulling off individual particles. We can conclude that whenever an agglomerate experiences a large acceleration, aerodynamically induced, dispersion will result. The force applied at C is particularly significant, in that there is insufficient time for reagglomeration to occur before the particles reach the collectors.

As can be seen in Fig. 2, knife-edges can be inserted into the flow-field at chosen points to define an arbitrary number of particle collectors. We have used 5 collectors in our research. The dividers are so oriented that particles enter the collectors without bouncing out — except of course for the small fraction that impinge directly on a knife-edge. To ensure that there is no upstream influence from the collectors on the flow in the separation zone, we ensure that each one "swallows" an undisturbed stream-tube that impinges on it. Thus the approaching stream lines remain straight and parallel, as illustrated in Fig. 2. To accomplish this, a venturi flow meter is positioned in each of the five discharge conduits to measure the flow, and a butterfly valve to control it. The discharge conduits each terminate in a filter bag that collects the particles. Of course, cyclones could be used instead for the larger particle sizes if preferred.

III. THEORETICAL RESEARCH

In order to effect quantitative design of the apparatus, and to predict cut points (d_{50}) and sharpness of cut values (β), one needs an analytical prediction of the particle trajectories. This is accomplished by generating a model of the flow-field through which the particles must pass, using a suitable law for aerodynamic drag, and computing the trajectories by numerical integration of the equations of motion.

3.1 Model of the Flow Field

Exterior to the region in the separation zone that is occupied by the feeder-jet air, the air velocity is simply and accurately modelled by $u_a = U$, a constant. Within the Coanda bend region, however, the velocity varies strongly with position. Based on the information contained in Ref. [6] and on our own measurements of velocity profiles, we have constructed the following velocity distribution (see Fig. 3). At each point $\{r, \theta\}$ for $0 \leq \theta \leq 90°$, the flow is perpendicular to $\underline{r}$ and has the magnitude $V_a(r, \theta)$. At each value of θ, the velocity profile has the shape shown in Fig. 4.

For $\xi \leq \xi_m$ (region I) we write

$$V_{a_I} = A\xi^2 + B\xi \tag{3.1}$$

and for $\xi_m \leq \xi \leq t'$ (region II) we write

$$V_{a_{II}} = u_m \operatorname{sech}^2[a(\xi-\xi_m)] + C[1-e^{-\lambda(\xi-\xi_m)}] \tag{3.2}$$

where

$$a = .88/(\xi_{m/2} - \xi_m) \tag{3.3}$$

In these equations, u_m, ξ_m, and t' have the values defined in Fig. 4, and A, B, C, u_m, ξ_m, $\xi_{m/2}$, λ and t are all functions of θ. These two equations contain the four parameters {A, B, C, u_m} which can be calculated as functions of $\{\xi_m, t', \lambda\}$ by imposing certain conditions:

$$V_{a_I} = V_{a_{II}} \quad \text{at} \quad \xi = \xi_m \tag{a}$$

$$\frac{dV_{a_I}}{d\xi} = \frac{dV_{a_{II}}}{d\xi} \quad \text{at} \quad \xi = \xi_m \tag{b}$$

$$V_{a_{II}} = V_E \quad \text{at} \quad \xi = t' \tag{c}$$

$$\int_0^{t'} V_a(\xi)d\xi = Q' \tag{d}$$

(3.4)

In these conditions, V_E is the external velocity at the edge of the Coanda region, and Q' is the volumetric flow through the section. These four conditions lead to a system of four linear algebraic equations that are solved numerically within the computing program. It remains to specify $\{\xi_m, \xi_{m/2}, \lambda, t', V_E, Q'\}$ as functions of θ to complete the model. These quantities are chosen as follows:

(i) We have made the arbitrary but reasonable assumption

$$V_E = U\sin\theta \tag{3.5}$$

(ii) Based on our measurements of velocity profiles, we have chosen

$$t' = t\left[1 + \left(\frac{r_i}{t} - 1\right)\frac{\theta}{\pi/2}\right] \tag{3.6}$$

(iii) Based on our own measurements, we have chosen to fit the variation of Q' with θ by

$$Q' = Q_F \left[1 + \frac{r_i \theta}{20t} \right] + V_E(t' - t) \qquad (3.7)$$

This equation models the entrainment of main flow into the feeder jet in its first term, and adds a contribution from the main flow by the second term. Here $Q_F = V_F t$, the volumetric flow from the feeder.

(iv) The data in ref. [6] in combination with our own results was used to generate expressions for ξ_m and $\xi_{m/2}$ as follows:

$$\xi_m = t'[.0833 + .4867e^{-5\theta}] \qquad (a)$$
$$\xi_{m/2} = t'[.5556 + .3194e^{-5\theta}] \qquad (b) \qquad (3.8)$$

(v) A value of λ that reasonably models the data is

$$\lambda = \frac{2}{t'} \qquad (3.9)$$

An example of the velocity field obtained with this model is shown in Fig. 5. This is for the case in which $V_F = U = 1.0$. The profiles, shown at 15° intervals, are seen to be quite reasonable. The model, in spite of the arbitrary features it contains, is considered to be entirely adequate for our purpose. (Compare with experimental results in Fig. 14 for $\theta = 90°$.)

3.2 Trajectory Calculations, and Theoretical β Values

The particle is acted on by two forces during its passage through the flow — gravity and aerodynamic drag. Gravity is relatively unimportant in the cases we are considering, and could have been neglected without significant loss of accuracy.

The aerodynamic drag is expressed as usual in terms of the drag coefficient C_D and the relative velocity $\underline{V}_r$,

$$\underline{D} = -C_D \frac{1}{2} \rho S \underline{V}_r |\underline{V}_r| \qquad (3.10)$$

The drag coefficient is a function of Reynolds number, and cannot be approximated adequately by Stokes' law for the ranges of Re encountered herein. An empirical fit that matches experimental data well for Re < 800 is:

$$C_D = \frac{24}{Re} (1 + .15Re^{.687}) \qquad (3.11)$$

where

$$Re = \frac{\rho d V_r}{\mu}$$

The first term of (3.11) represents Stokes' law, and is only valid for $Re < 1$.

The equations of motion of a particle are most conveniently formulated in polar coordinates when it is inside the Coanda region, and in Cartesian coordinates after it has emerged. The corresponding sets of equations are (see Fig. 3 for coordinate systems)

Cartesian:

$$m\ddot{x} = C_D \frac{1}{2} \rho S |V_r| (U - \dot{x})$$

$$m\ddot{y} = mg - C_D \frac{1}{2} \rho S |V_r| \dot{y} \tag{3.12}$$

where

$$|V_r| = [(U - \dot{x})^2 + \dot{y}^2]^{1/2}$$

and $\{x, y\}$ are the coordinates of the particle.

Polar:

$$m(\ddot{r} - r\dot{\theta}^2) = -\frac{1}{2} C_D \rho S |V_r| \dot{r} + mg \sin\theta$$

$$m(r\ddot{\theta} + 2\dot{r}\dot{\theta}) = \frac{1}{2} C_D \rho S |V_r| (V_a - r\dot{\theta}) + mg \cos\theta \tag{3.13}$$

where

$$|V_r| = [\dot{r}^2 + (V_a - r\dot{\theta})^2]^{1/2}$$

and $\{r, \theta\}$ are the coordinates of the particle, and V_a is given by either (3.1) or (3.2) depending on the values of $\{\theta, \xi\}$.

Equations (3.12), (3.13) were converted to first-order form and programmed for digital computation using a Runge-Kutta second-order numerical integration. A typical set of trajectories is shown in Fig. 2 for a range of spherical particles. Many such trajectories were examined, with varying values of the parameters, in order to select the geometry of the separation zone and knife-edges.

There are two major factors that can cause the real trajectories to depart from those shown and hence to degrade the performance. These are the initial position of the particle in the exit slit (it can be anywhere within the range $0 \leq \xi \leq t$) and its initial velocity, both magnitude and direction, may deviate from the nominal. By allowing for variation of these parameters in the computation, we can study the "spread" of the trajectories associated with these two effects, as illustrated in Figs. 6, 7, 8. Figure 6 shows the effect of initial position for a 40 μm particle. It is evident that position variation is a minor source of error for this size of particle. This is a generally valid conclusion for very thin slits, but for wider slits, initial position can be a significant source of error. Figure 7 shows how a variation in the initial direction of the particle can influence its trajectory. For the 40 μm particle, there is little ambiguity at the collector knife edge, but the 80 μm particle shows significant dispersion. This effect can be suppressed by designing the feeder duct to produce a parallel flow of particles. Figure 8 shows the most important source of trajectory perturbations, variation in particle entry speed, in this case by ±20% from the mean. This causes a significant dispersion of the trajectories. Since the velocity profile of the feeder air at the exit slit cannot be uniform, the variation in particle speed may well be linked to position. Thus the effects shown in Figs. 6, 8 are combined in Fig. 9, in that the particle entry speed depends on position, being lowest near the walls and highest at the centre. The spread in the trajectories does not appear to be much worse than in Fig. 8, but in fact when all particle sizes are considered, and especially for wider slots, the sharpness of cut obtained is appreciably less when velocity error and position error are combined than for either one alone.

From computations of trajectories such as those illustrated above it is possible to predict the cut point, d_{50}, and the sharpness of cut, $\beta = d_{25}/d_{75}$, insofar as the variations in initial position and velocity are responsible for grade efficiencies departing from the ideal. This is accomplished by assuming that it is equally probable for a particle to start from any point in the entry slit, and assigning a velocity distribution $V_p(\xi)$ at the slit. A large number of trajectories are then computed for one particle diameter, for equally spaced intervals at the entry slit, and the number of particles entering each collector is counted. This yields a set of coarse grade efficiencies $\eta_i(d)$, $i = 1...4$, corresponding to the four knife edges. Repeating this procedure for many diameters yields curves of $\eta(d)$ for each knife edge, and hence values of d_{50} and β. One such representative curve is shown in Fig. 10. The resulting β values are plotted vs. d_{50} in Fig. 11. Curve A shows the influence of slot thickness alone, and it is seen that β values greater than 0.93 can be achieved if the entry velocity is uniform. Curves B and C show the performance calculated when the particle velocity distribution across the slit is parabolic, mimicking the air flow velocity distribution. The values $\sigma = .1$ and .3 represent the range that may realistically be expected in a good design. This figure clearly shows that variations of particle velocity away from the mean can be a major cause of non-ideal performance. Indeed, we have concluded that it is the primary cause in our apparatus, and that an optimum design of separator demands that this variation be kept as small as possible.

IV. EXPERIMENTAL RESEARCH

The experiments we carried out are of four main kinds:-

(i) aerodynamic measurements to establish the properties of the flow,

(ii) measurements of η, d_{50} and β for glass spheres of specific gravity about 2.4, and of various size distributions,

(iii) separations of various non-spherical powders,

(iv) measurements of the particle velocity distribution at the feeder slit.

These experiments are described in the following sections.

4.1 Velocity and Turbulence Measurements

Measurements of mean air velocity and turbulence were made with a hot-wire anemometer at the entrance to the separation zone, at the feeder slit, and at several stations inside the Coanda flow region. A single wire was used, normal to the mean flow, so that only the streamwise component of turbulence was measured.

The profiles at the exit of the contraction, i.e., at the entrance to the separation zone (see Fig. 1) are shown in Fig. 12. Figure 12(a) shows those for the horizontal centreline, and 12(b) those for the vertical centreline. It is clear that the velocity outside the wall boundary layers is very uniform, and that the rms turbulence is of the order of 1/2%. The flow into which the particles are injected for subsequent separation is therefore of excellent uniformity and steadiness.

The flow from the feeder slit was measured just downstream of its exit, midway along its length. In this experiment, the feeder duct was removed from the separator, and the jet was allowed to discharge into free air. The results are shown in Fig. 13. The velocity distributions and turbulence are typical of those to be expected of a jet emerging into still air. It is noteworthy that the velocity distributions are characteristic of a turbulent pipe flow, rather than laminar (which would display a parabolic velocity distribution). The turbulence is seen to be quite moderate at the centre of the jet, and characteristically high in the mixing zones at its edges. Figure 13 serves only to give insight into the feeder duct performance upstream of the entry slit. Conditions inside the separation zone in the presence of the Coanda bend and the separation air flow do not of course correspond to those in the free jet.

The conditions near the upper surface of the separation zone, downstream of the Coanda bend, are shown in the next series of figures. Figure 14 shows the velocity profiles at $x = 0$ (see Fig. 3), i.e. at the termination of the Coanda bend, for three cases - jet speed equal to 1/2, 1.0, 2.0 times the main flow speed. (Compare with Fig. 5 for ratio = 1.0.) Figure 15 shows these profiles farther downstream at about $3r_j$, and Fig. 16 shows the turbulence profiles at the same location. The layer affected by the feed air, after being turned 90° by the Coanda effect, is quite thin, using the turbulence data of Fig. 16 as a criterion. It is also abundantly clear that the Coanda effect exists, in that the main flow below this layer remains unaffected by the feeder jet. There is a substantial difference between the three cases shown, in that the disturbance to the main flow is much greater when the feeder jet velocity exceeds that of the main flow.

4.2 Measurements of η and β for Glass Spheres

To measure coarse grade efficiency (η) and sharpness of cut (β), we separated a variety of glass sphere mixtures in the EPS. In most of these experiments, we weighed the material collected in each collector bag, took samples for photographic analysis, measured the diameter distributions from the photographs, and then computed values of η and β. A sample photograph is shown in Fig. 17, and a sample graph of η in Fig. 18. The results for β from a large number of runs under varying conditions of velocity and feed rate and with different configurations of solids feeder and feeder air duct are shown in Fig. 19. Also shown for comparison are two theoretical curves from Fig. 11. It is clear that the experimental results show reasonable concordance with the theory. The scatter of the measurements is to be expected: this is a difficult measurement to make and is subject to considerable statistical variability, not only in the physical conditions present in the test but also in the sampling and analysis procedures. We think it is fair to conclude that at the smallest diameters the scatter in particle velocity at the entry to the separation zone is large, with σ of order 0.3-0.4, whereas the larger particles probably had narrower speed distributions, with σ = 0.1 or less. These inferences are supported by the experiments on particle velocity (see below).

Part of the scatter in Fig. 19 results from variation in the feed rate. Figure 20 shows values of β measured for glass spheres with d_{50} between 25 and 50 μm over a wide range of feed rate. The maximum rate corresponds roughly to 1/2 tonne per hour in the laboratory apparatus. The value of β is consistently larger than 0.7, and decreases slightly with increasing feed rate.

4.3 Measurements of Particle Velocity

Because we inferred from the theoretical results that the particle velocity distribution plays a crucial role in determining the sharpness of cut, we made measurements of this distribution to try to gain an understanding of what physical and geometrical effects govern it.

The technique used was to make transparent glass duct walls and to position a camera and floodlight so that the particles could be photographed in flight. A shutter was constructed of a rotating disc with a wedge-shaped slit, that was interposed between the camera and the duct. The resulting photographs yield a streak for each particle in focus, the length of which is proportional to the particle speed. By measuring the lengths of many streaks, we were able to construct histograms of particle speed and calculate a normalized standard deviation $\sigma = \sigma/V_p$. We did numerous experiments, with different bead sizes, different feeder air speeds, and different duct thicknesses. A representative set of results is shown in Fig. 21. The measure of scatter here is σ = .21. The physical mechanism responsible for so wide a speed range has not been conclusively identified, but we have strong evidence that it relates to triboelectric effects [8]. We measured a substantial voltage on the walls of an insulated steel feeder duct that increased with solid mass flow rate, and a current to ground from an electrode in the wall that likewise increased. This indicates that charge exchange takes place somewhere in the system. Our tentative conclusion is that charged particles interact with the duct wall and are slowed down. Small particles may even come to rest on the wall. Our experiments show that increasing the air speed and increasing the duct wall separation are both beneficial in reducing σ. We also observed that the value

of σ is smaller for larger particles. All three of these effects (speed, duct thickness, particle size) are consistent with the triboelectric explanation. It remains a major challenge to reduce σ to less than 0.1 for the smallest particles, and our current research is directed to this goal.

4.4 Integrity of the Coanda Flow

It was anticipated that at some unknown level of feed rate, the solid fraction of the feeder flow would have sufficient momentum to cause a major separation of the gas fraction from the Coanda bend. Evidence of this phenomenon might be a downward shift of the trajectories of the particles. To observe whether this occurred within the test range, we calculated the "mean collector" by the expression

$$\bar{c} = \sum_{1}^{5} n \cdot w_n / \sum_{1}^{5} w_n$$

where w_n is the weight in collector n. If the expected separation took place, one should see a reduction in $\bar{c}$, as more of the particles arrived in collectors 1 and 2, and fewer in 4 and 5. The result is shown in Fig. 22. It can be seen that there is no evidence of any reduction in $\bar{c}$. Thus either $\bar{c}$ is not a good indicator of flow separation, or none took place up to a feed rate of 8 kg/m. The latter conclusion is tentatively accepted; more detailed aerodynamic measurements need to be made, and higher feed rates need to be provided in order to arrive at a definitive conclusion. This aspect of the research is thus incomplete.

4.5 Separation of Other Materials

The EPS has been used to separate other materials representative of industrial applications. Typical results are illustrated in the micro- photographs shown in Figs. 23, 24, for samples of carbon and cement. Figure 25 shows the size distributions of the feed and of the five products, for the cement of Fig. 24. The result shows excellent separations.

The sharpness of cut values for separations of cement at various feed rates are shown on Fig. 26. They fall off more rapidly than those for glass beads in a similar size range (Fig. 20), the useful maximum being about 2 kg/min for this apparatus. It is tentatively hypothesized that this results from the presence of a much larger proportion of fines in the cement than in the glass, resulting in both more agglomeration, and a higher level of aerodynamic interference between particles.

In other applications, we have found good separation of binary mixtures in which the two components have different terminal velocities.[4] These include fly ash, and ground mica ore.

---

[4] Although the EPS does not utilize terminal velocity per se as a basis of separation, nevertheless, the factors that control terminal velocity, i.e., size, density and shape, are the same ones that govern particle trajectories in the EPS. Thus the EPS and the TERVEL separator are similar in that they distinguish between particles on a similar basis.

V. CONCLUDING REMARKS

Research carried out in support of the development of the EPS, an aerodynamic particle separator, has verified that the flow field in the separation zone is uniform, steady and undisturbed by the feeder air, which is confined to a narrow zone adjacent to the Coanda bend and the upper surface of the separation zone. Particle distributions in the collectors, and measured values of η and β verify that the theoretical predictions concerning particle trajectories, and performance of the separator are borne out in practise. High performance down to small particle size depends on (i) good particle dispersion, (ii) the existence of a uniform steady flow in the separation zone, and (iii) uniform entry speed of the particles at a narrow slit.

Future research should be directed at reducing agglomeration, improving the uniformity of particle velocity at entry to the separation zone, and to establishing the upper limit to the feed rate.

REFERENCES

1. S. Raimondo, A. A. Haasz, B. Etkin, "The Development of a Horizontal Elutriator-Infrasizer MK III", UTIAS Report No. 235, March 1979.

2. A. H. von Flotow, B. Etkin, "Performance of the University of Toronto Infrasizer MK III as a Monosizer and Multi-Cut Classifier", Powder Technology, 30, 1981, pp. 257-264.

3. H. Rumpf, Diss., T. H. Karlsruhe, 1939.

4. K. Leschonski, "Das Klassieren disperser Feststoffe in gas formingen Medien", Chem. Eng. Tech., 49, 1977, pp. 708-719.

5. H. Rumpf, K. Leschonski, "Method of an Apparatus for Sifting Particulate Material in a Cross-Current", U.S. Patent 4,132,634, Jan. 2, 1979.

6. B. G. Newman, "The Deflexion of Plane Jets by Adjacent Boundaries — Coanda Effect", in Boundary Layes and Flow Control, Pergamon Prss 1961, pp. 232-262.

7. S. Horvath, "Theoretical Design of Contraction Ducts for Two-Dimensional Wind Tunnels", University of Toronto, B.A.Sc. Thesis, April 1983 (unpublished).

8. B. Etkin, "Research on a Novel Particle Classifier", Final Report to NSERC on PRAI Grant No. P-8212, Nov. 1985 (unpublished).

9. A. Suganuma, H. Yamamoto, R. Aoki, "Pneumatic Dispersion and Classification of Fine Powders", in Powder Technology, the Proceedings of International Symposium on Powder Technology, Kyoto Japan, 1981, pp. 742-749, Hemisphere Pub. Corp., New York.

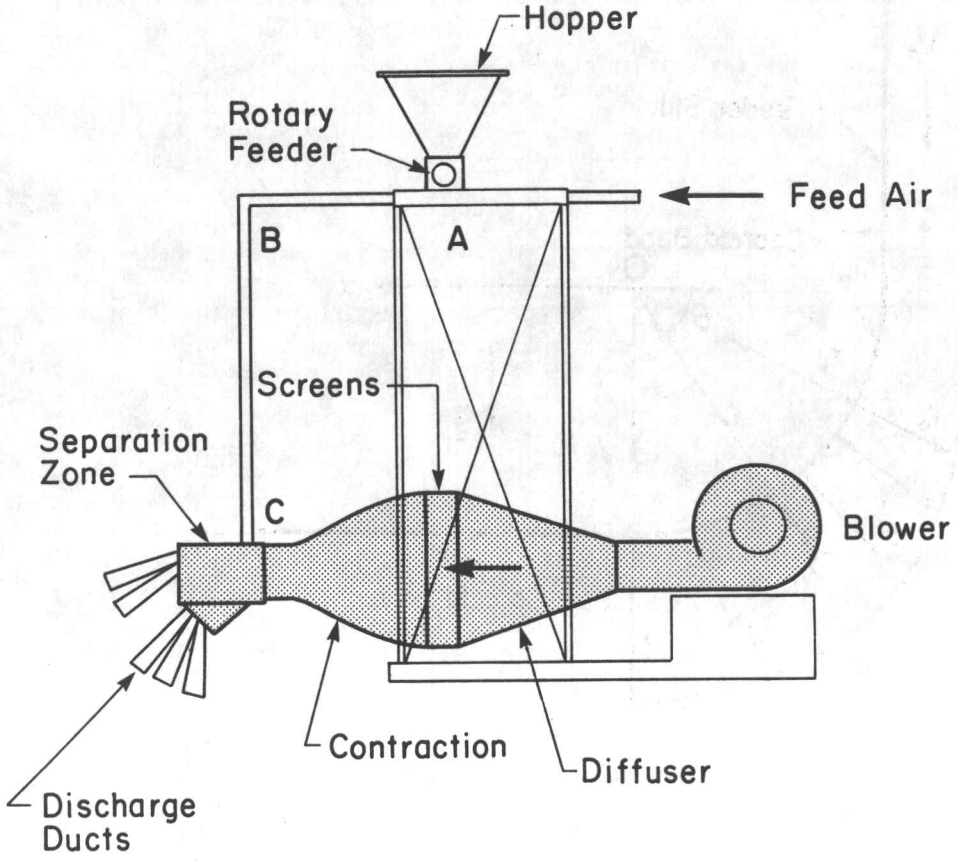

FIG. 1 GENERAL ARRANGEMENT OF EPS

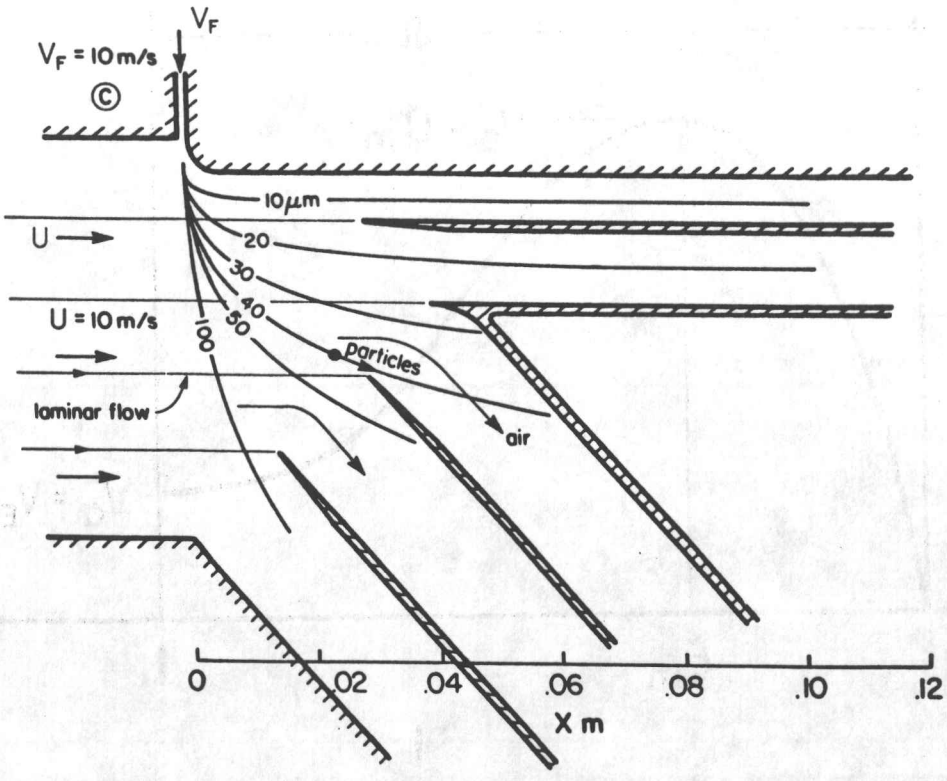

FIG. 2 SEPARATION ZONE IN THE EPS

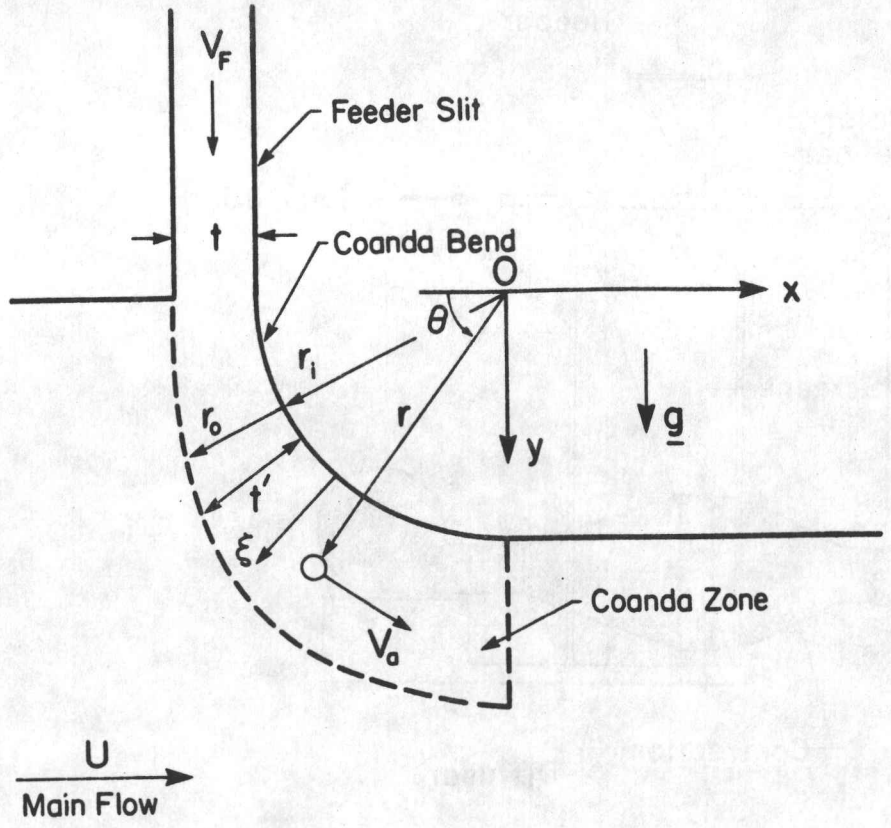

FIG. 3 DEFINITIONS FOR COANDA FLOW

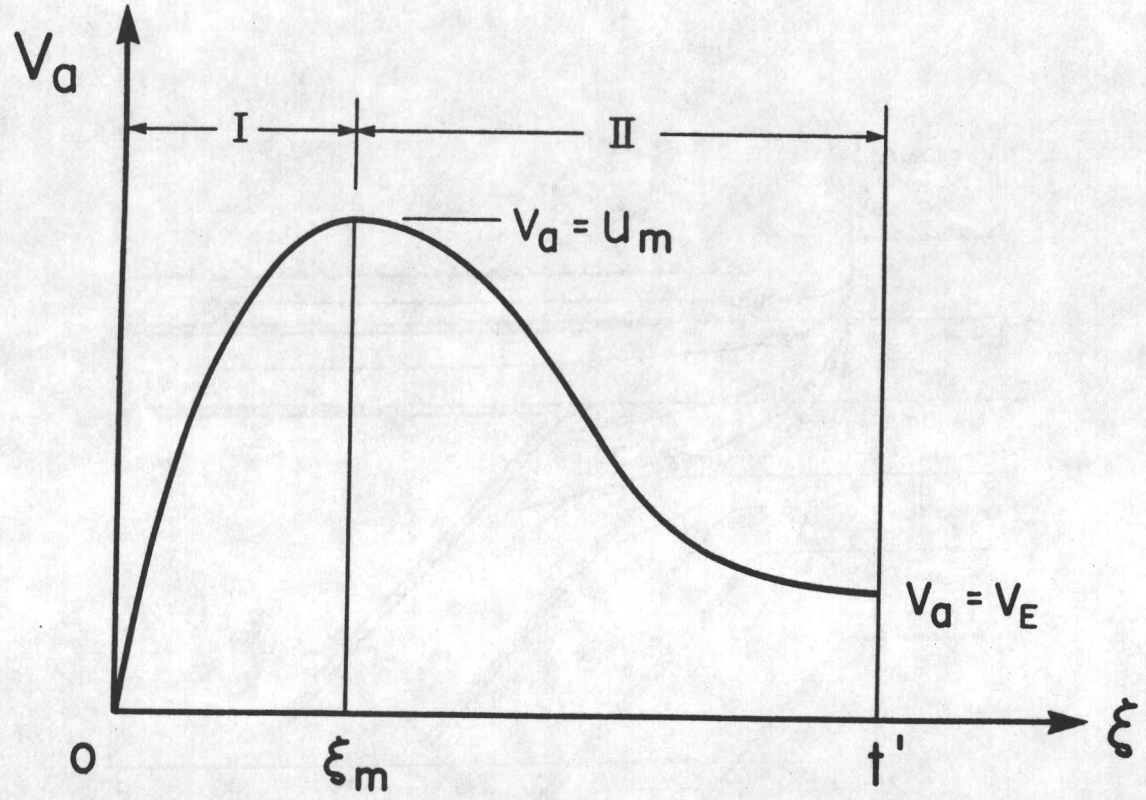

FIG. 4 VELOCITY PROFILE IN THE COANDA ZONE

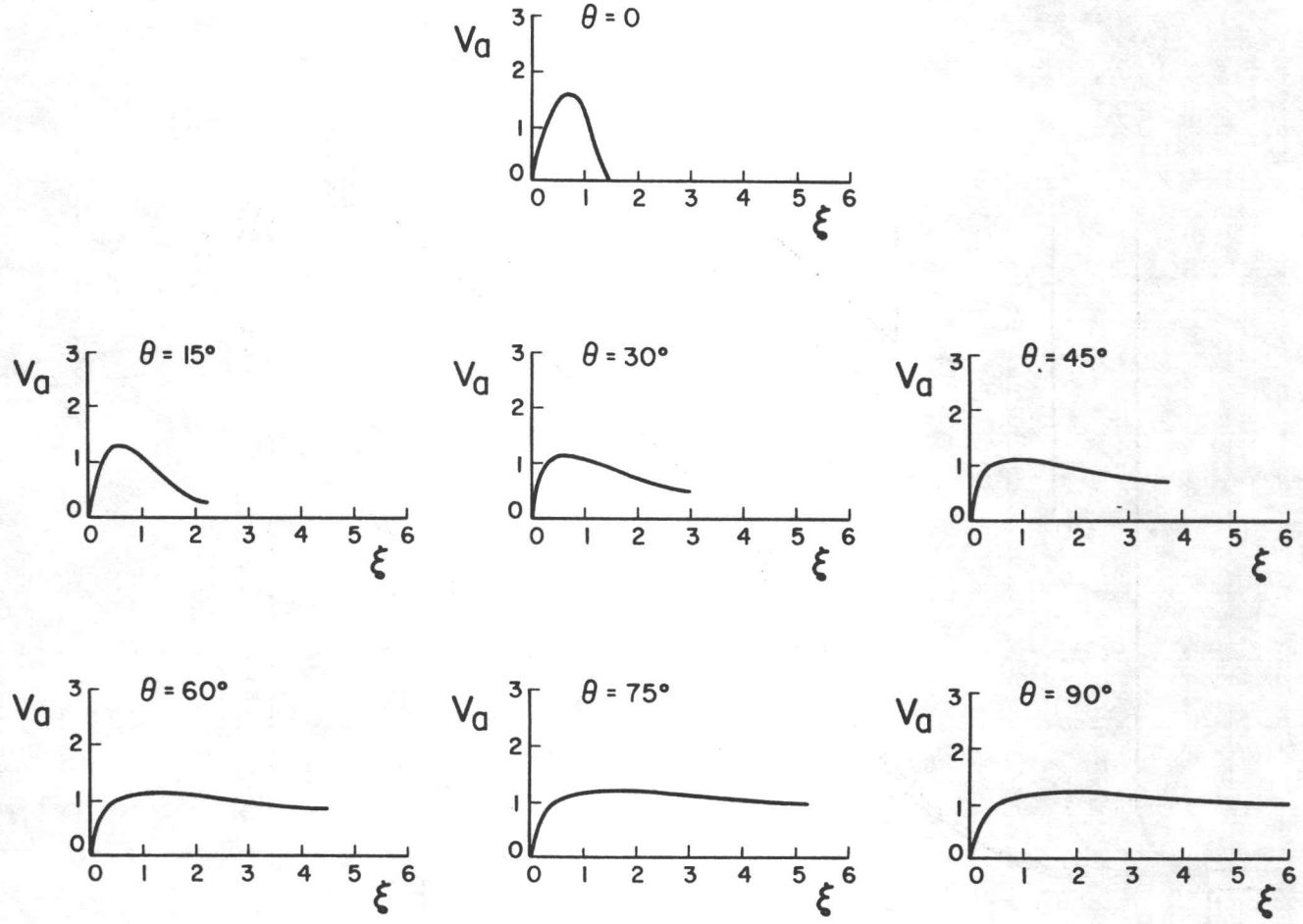

FIG. 5 SAMPLE VELOCITY PROFILES OF THE MODEL USED
$t = 1.5$ mm, $r_i = 6.0$ mm, $U = V_F = 1.0$

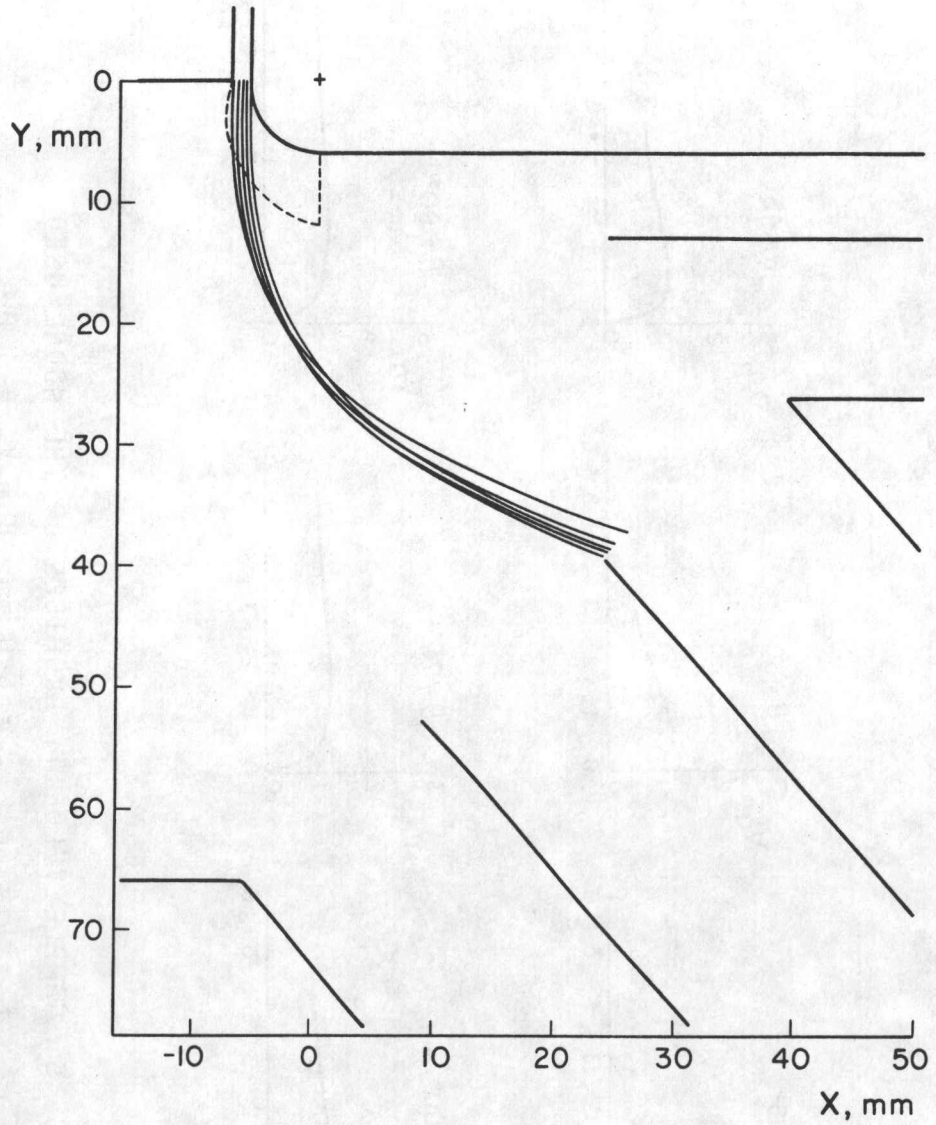

FIG. 6 EFFECT OF INITIAL POSITION ON TRAJECTORY

s.g. = 2.0, d = 40 μm, t = 1.5 mm, r_i = 6.0 mm

V_{p_o} = U = V_F = 10 m/s

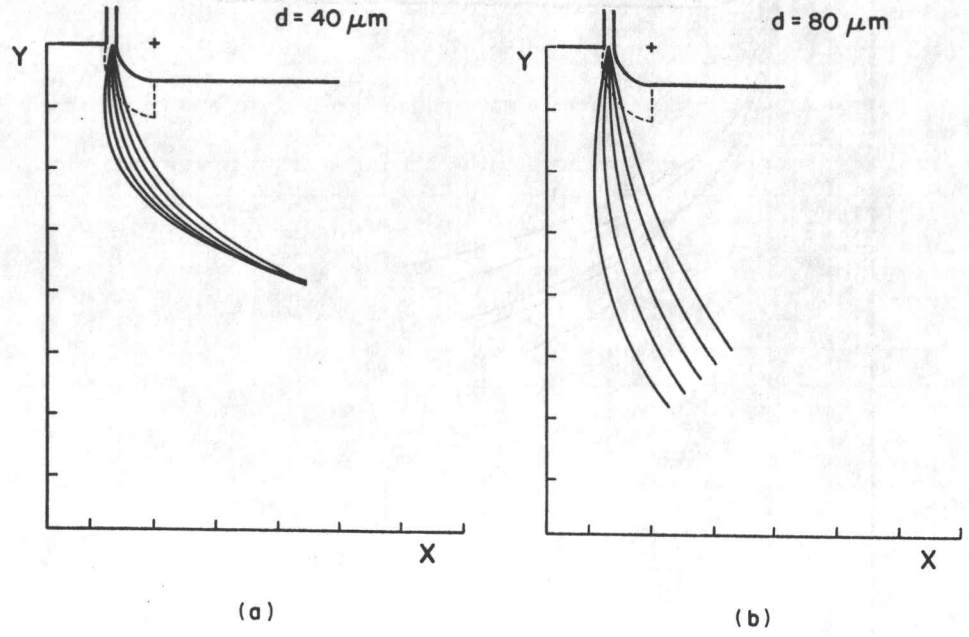

FIG. 7 EFFECT OF INITIAL DIRECTION ON TRAJECTORY
s.g. = 2.0, t = 1.5 mm, r_i = 6.0 mm
V_{p_o} = U = V_F = 10 m/s

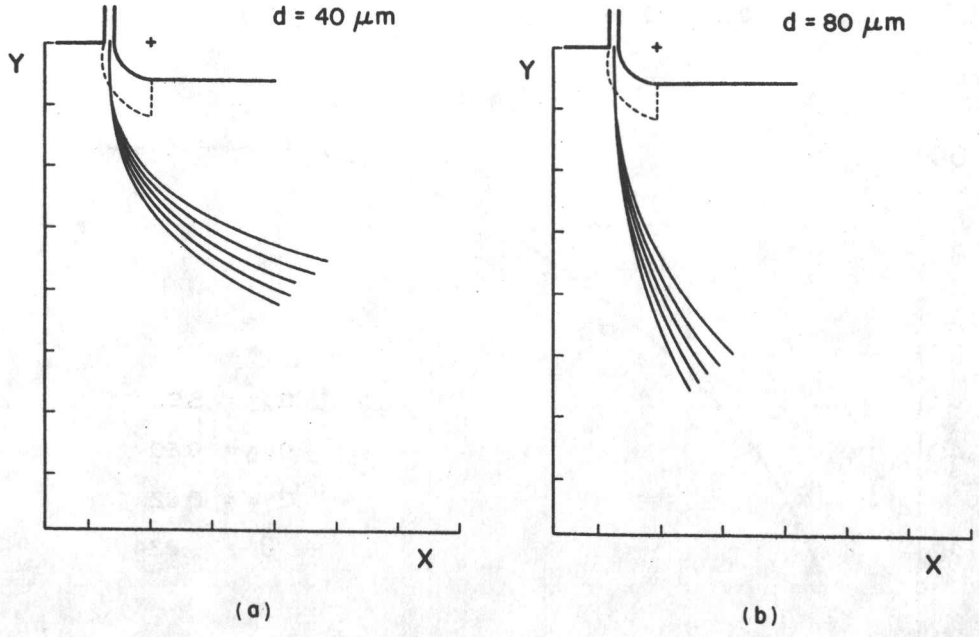

FIG. 8 EFFECT OF INITIAL SPEED ON TRAJECTORY
s.g. = 2.0, t = 1.5 mm, r_i = 6.0 mm
U = V_F = 10 m/s, 8 ≤ V_{p_o} ≤ 12 m/s

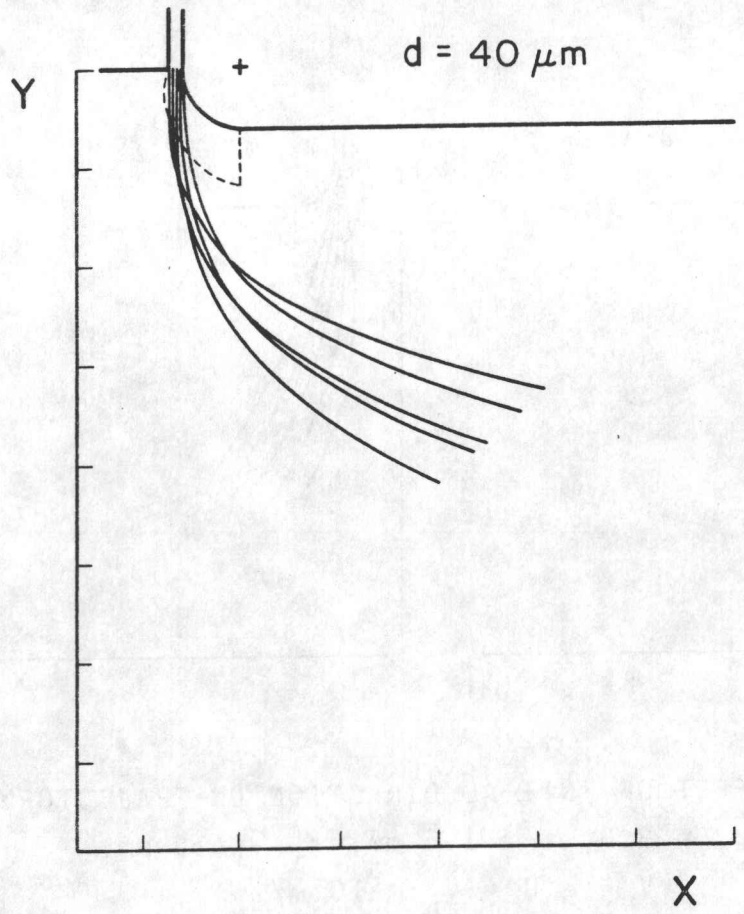

FIG. 9 EFFECT OF COMBINED SPEED/INITIAL POSITION ON TRAJECTORY
s.g. = 2.0, d = 40 μm, t = 1.5 mm, r_i = 6.0 mm
U = V_F = 10 m/s, 8 ≤ V_p ≤ 12 m/s

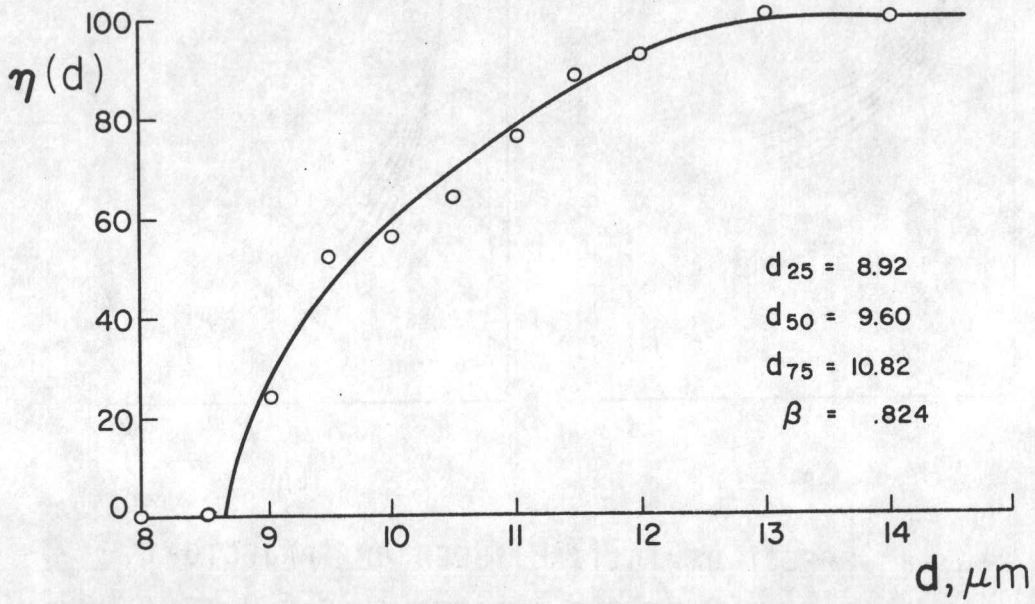

FIG. 10 THEORETICAL COARSE GRADE EFFICIENCY
V_F = U = 10, $\hat{\sigma}$ = .36
CUT AFTER COLLECTOR NO. 4

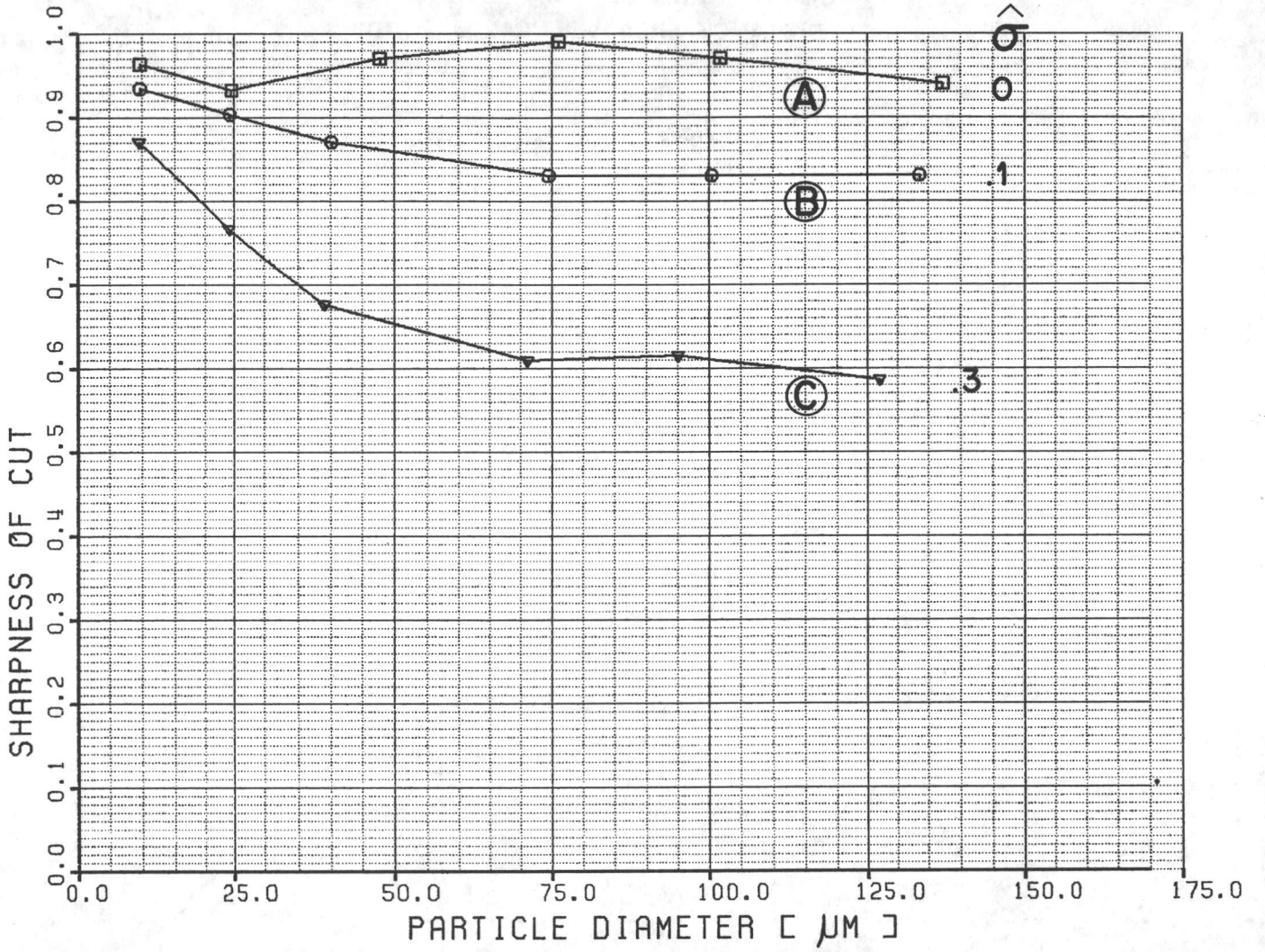

FIG. 11 THEORETICAL VALUES OF β

$\bar{v}_p = V_F = U = 10$ m/s

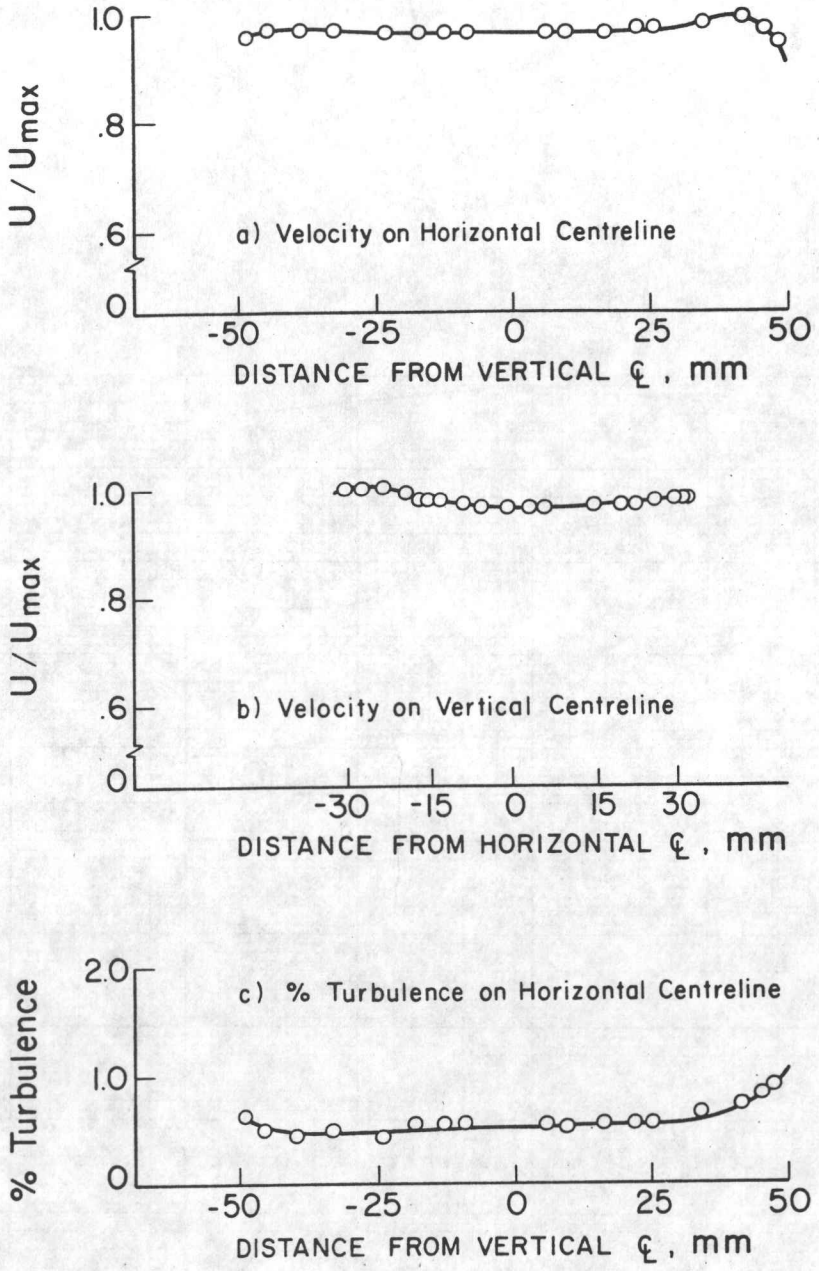

FIG. 12 AIR VELOCITY PROFILES AT ENTRANCE TO SEPARATION ZONE.

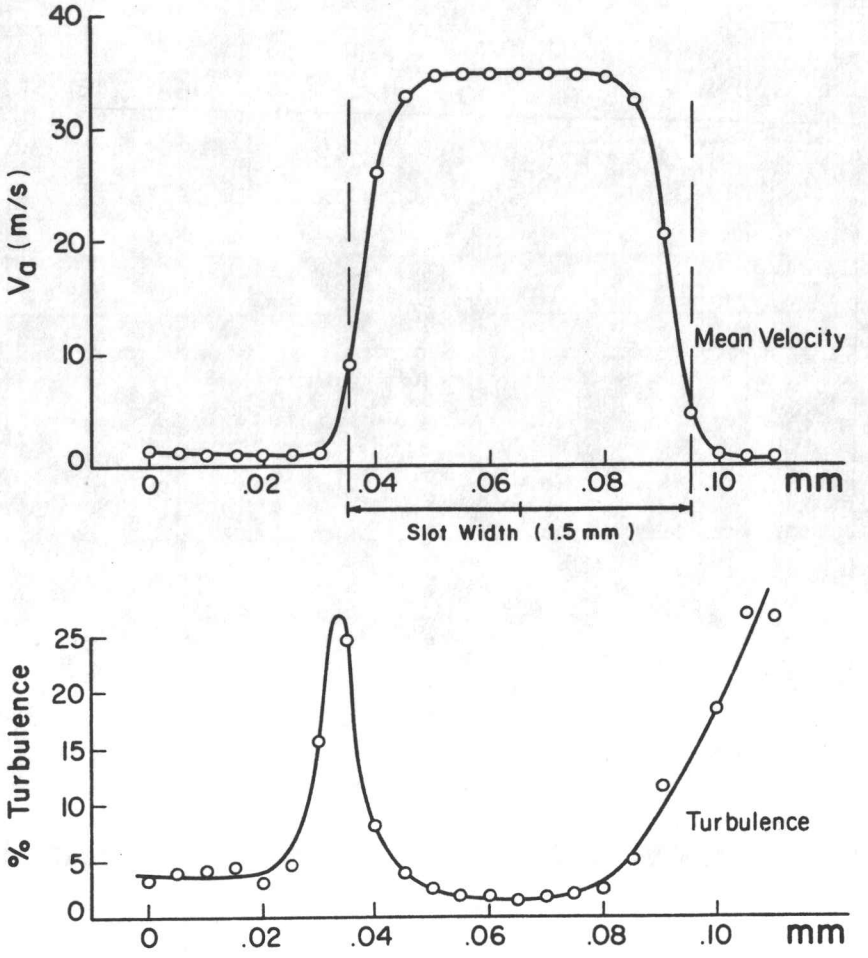

FIG. 13 AIR VELOCITY PROFILE AT EXIT OF FEEDER DUCT

V_F = 30 m/s

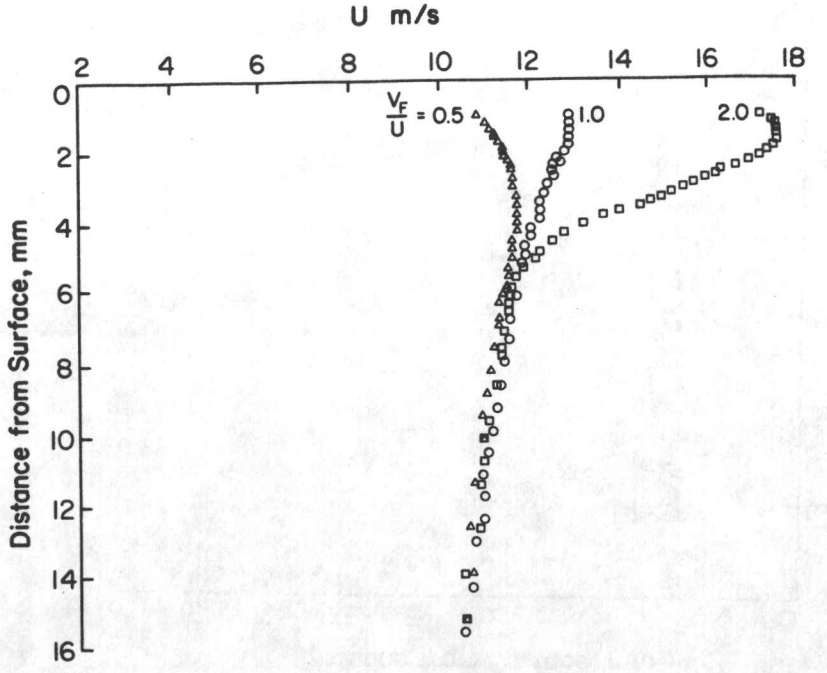

FIG. 14 MEAN-VELOCITY PROFILES IN SEPARATION ZONE

X = 0

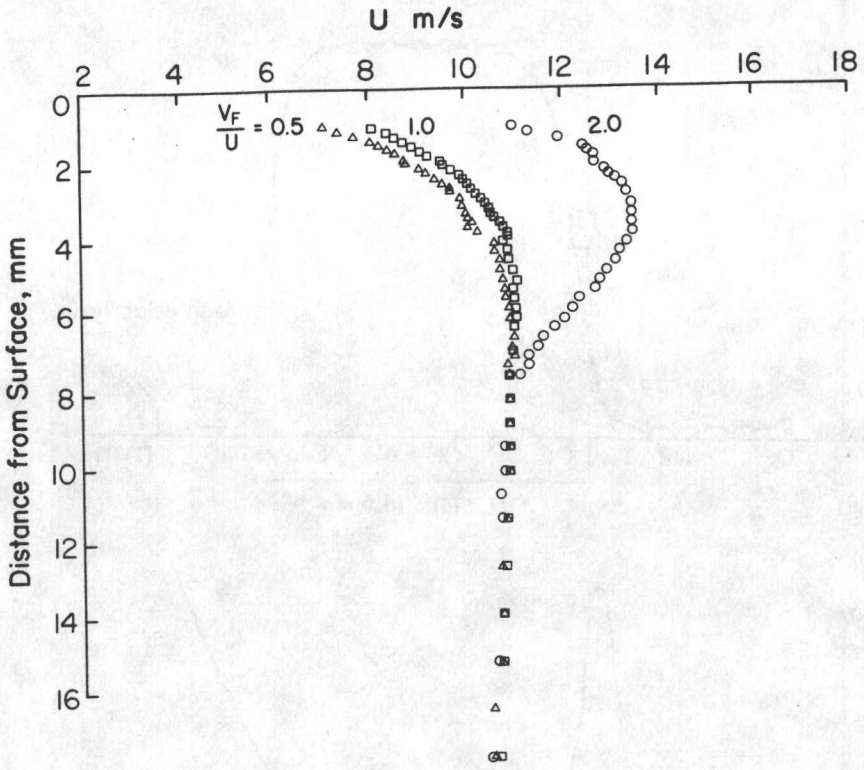

FIG. 15 MEAN-VELOCITY PROFILES IN SEPARATION ZONE
X = 19 mm

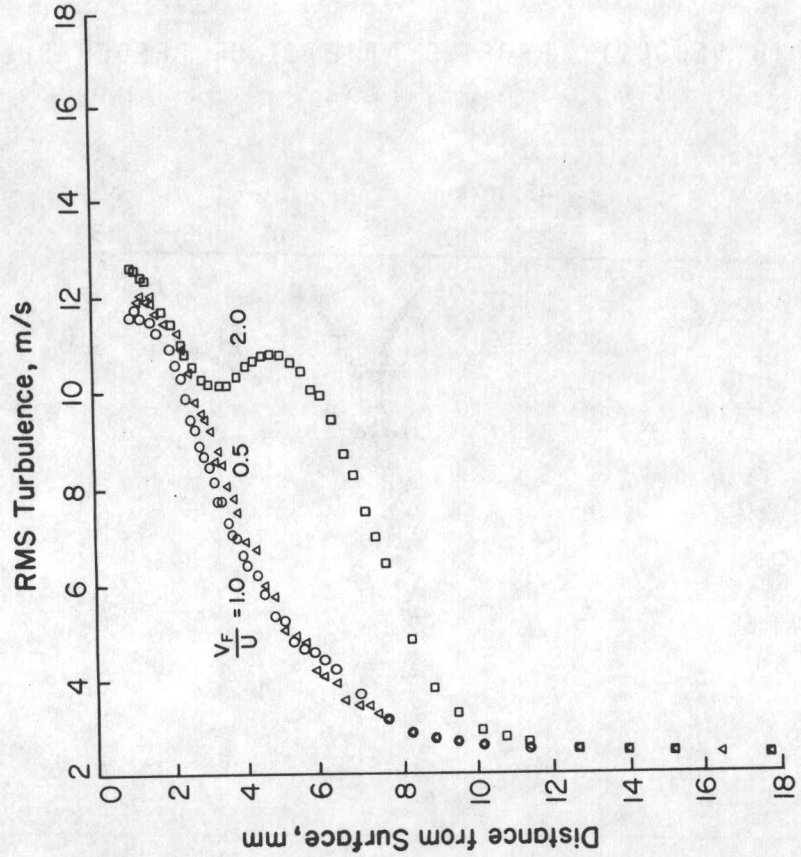

FIG. 16 TURBULENCE PROFILES IN SEPARATION ZONE
X = 19 mm

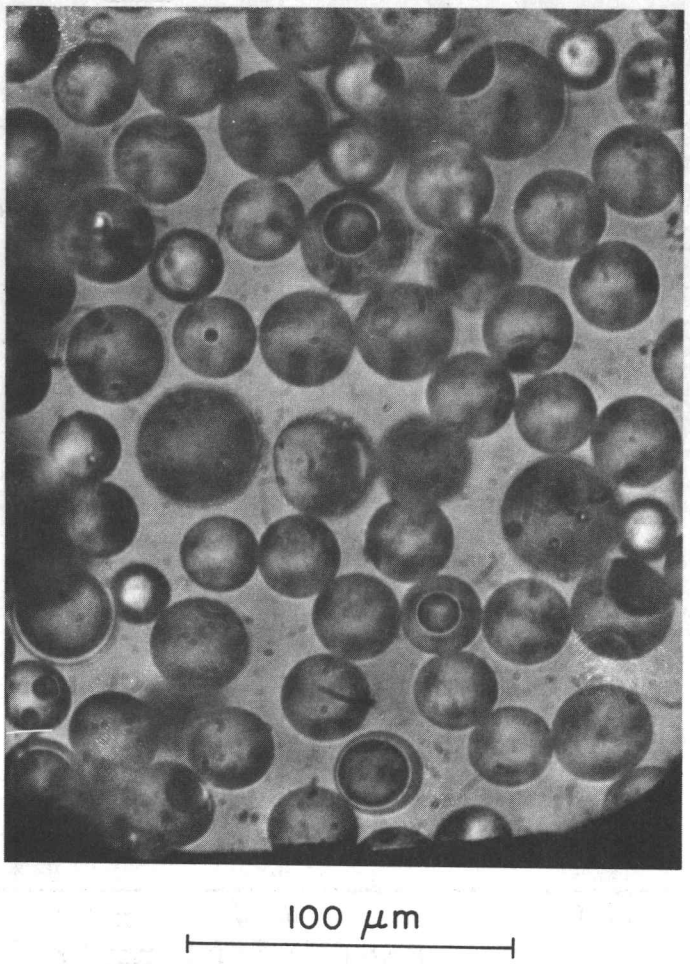

FIG. 17 SAMPLE PHOTOGRAPH
GLASS SPHERES, COLLECTOR #3

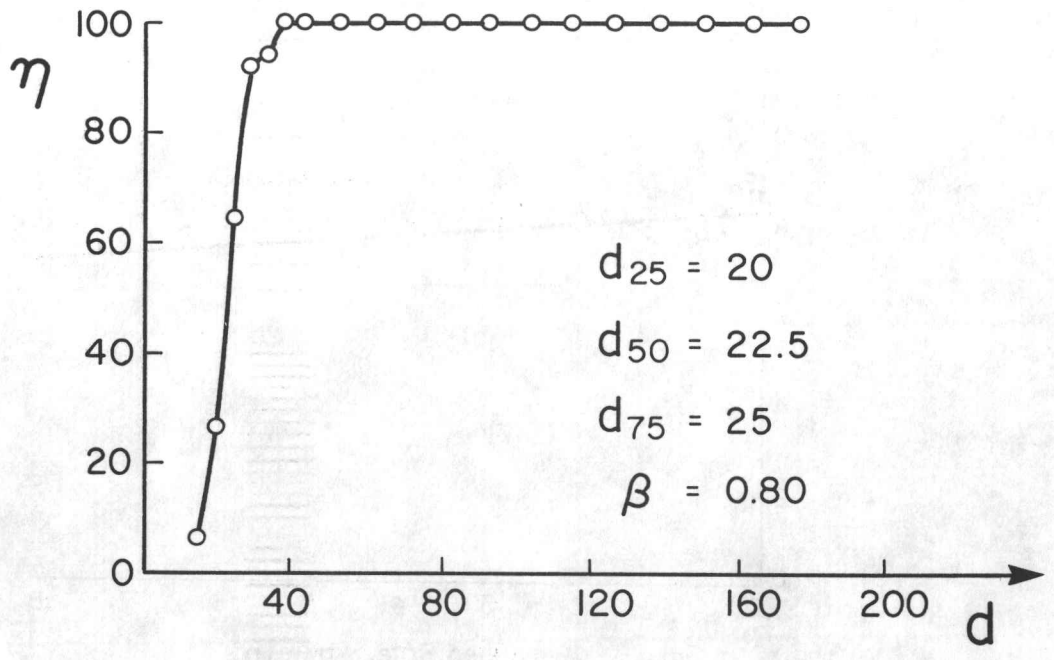

FIG. 18 SAMPLE OF MEASURED COARSE GRADE EFFICIENCY
CUT AFTER COLLECTOR #3

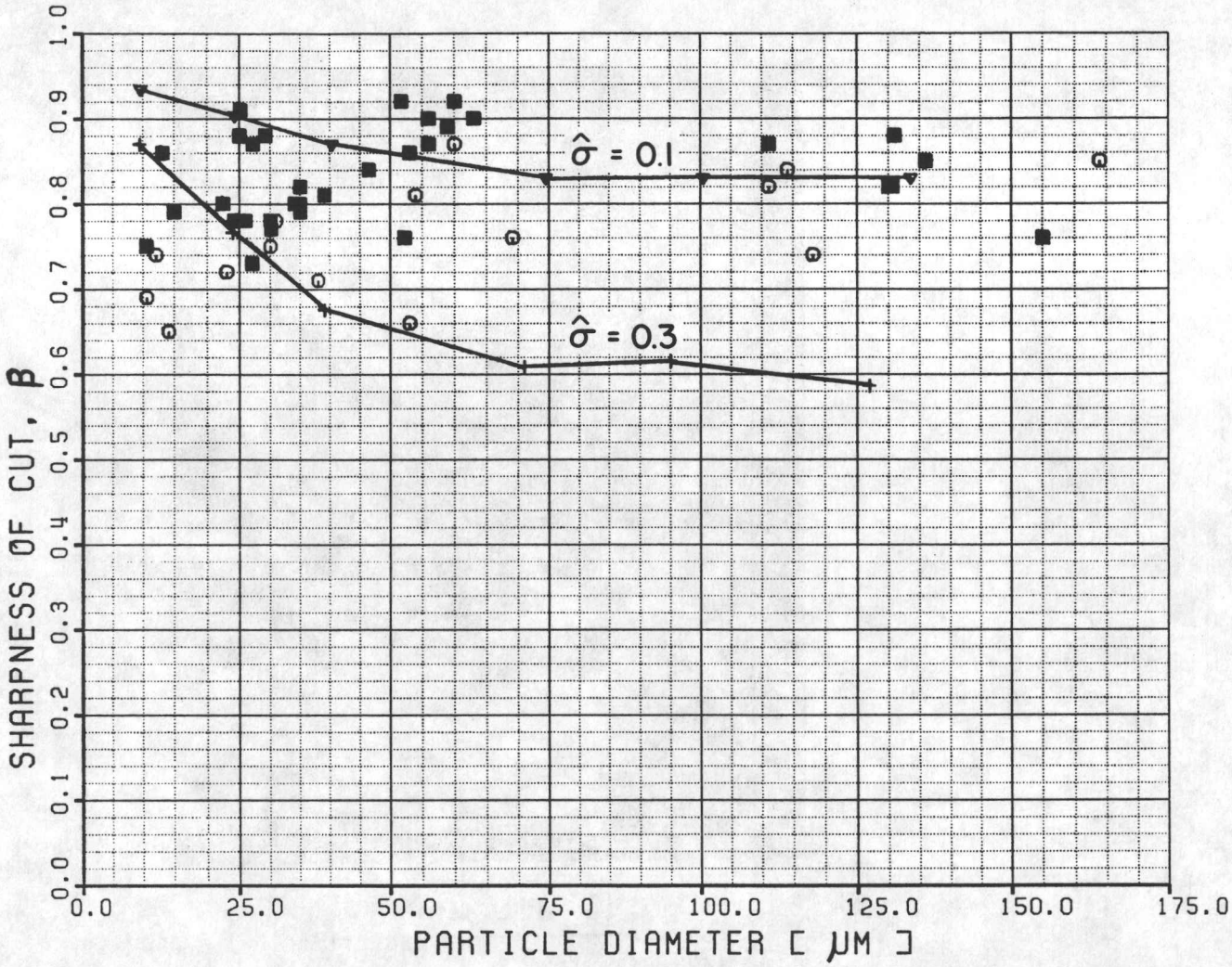

FIG. 19 MEASURED SHARPNESS OF CUT
SAMPLE: GLASS BEADS; MASS FLOW RATES

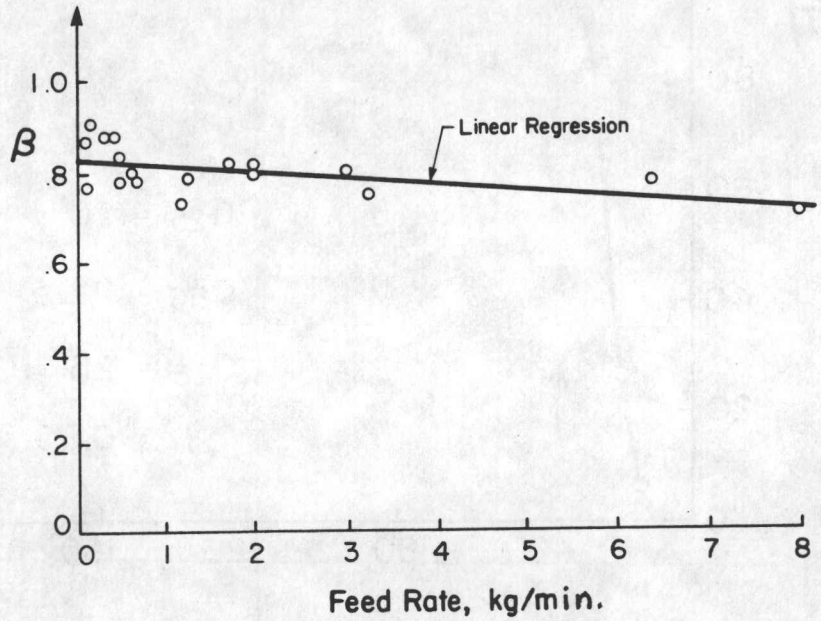

FIG. 20 MEASURED SHARPNESS OF CUT, GLASS SPHERES,
$25 < d_{50} < 50$ μm

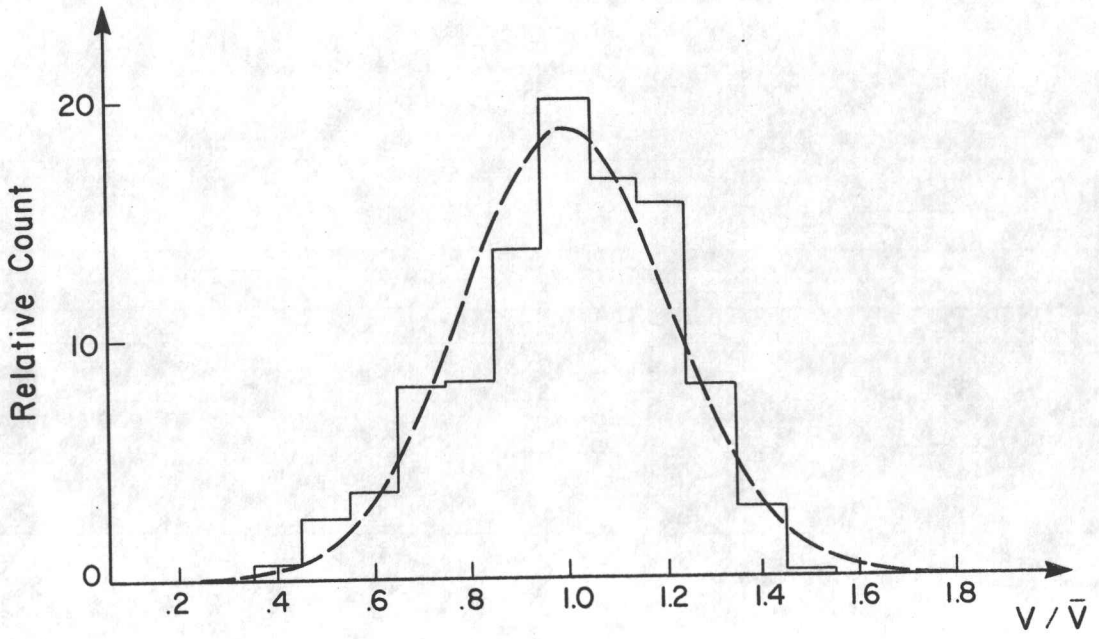

FIG. 21 HISTOGRAM OF PARTICLE VELOCITY
GLASS SPHERES; 28 ≤ d ≤ 53 μm
V_F = 20 m/s

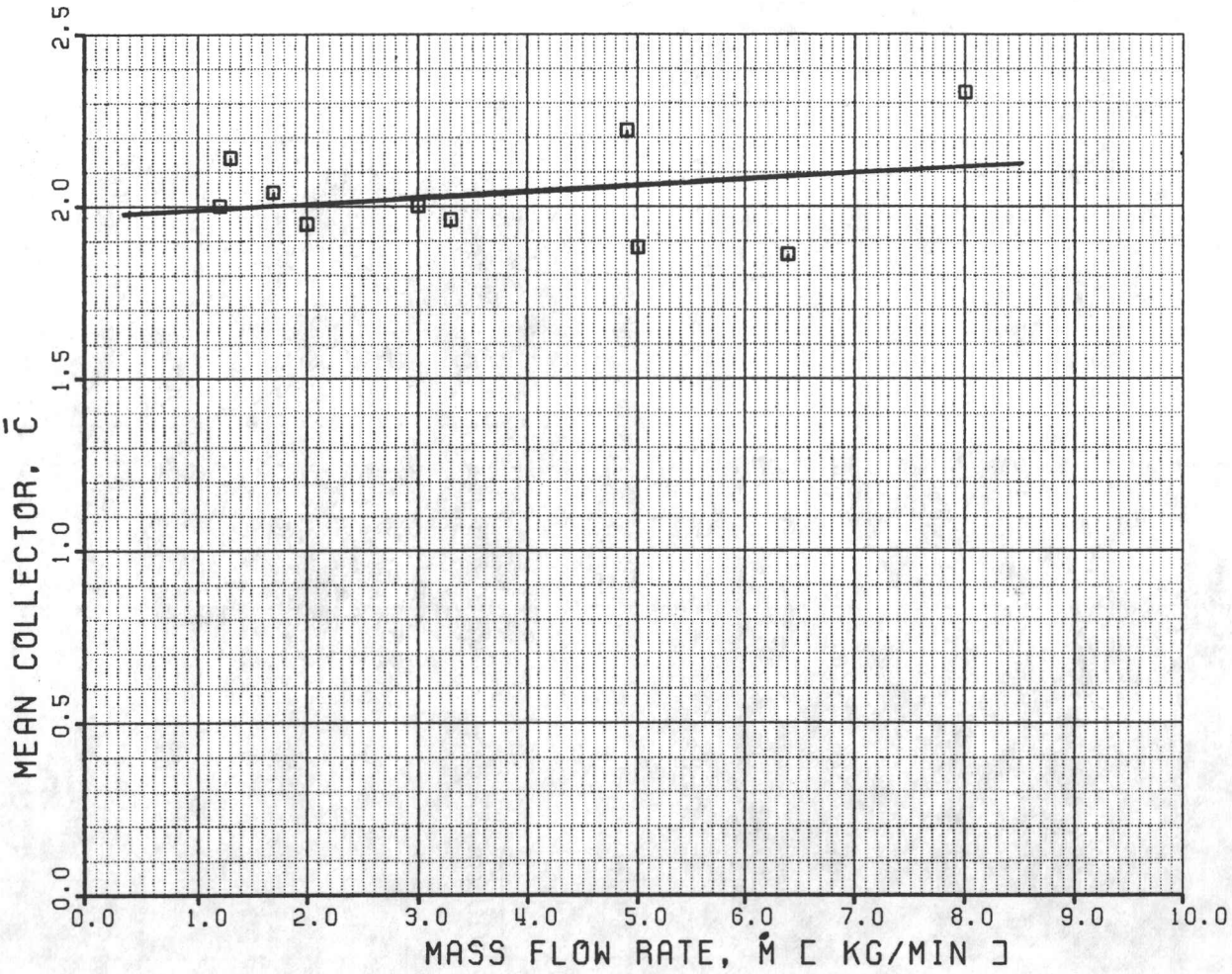

FIG. 22 VARIATION OF $\bar{c}$ WITH MASS FLOW

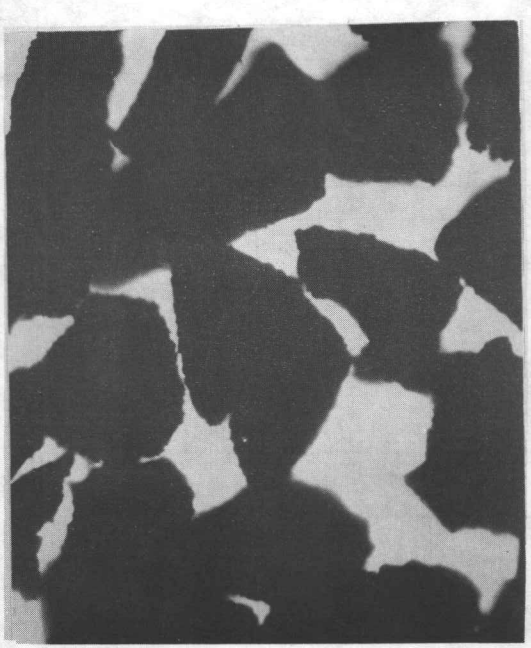

Collector #1

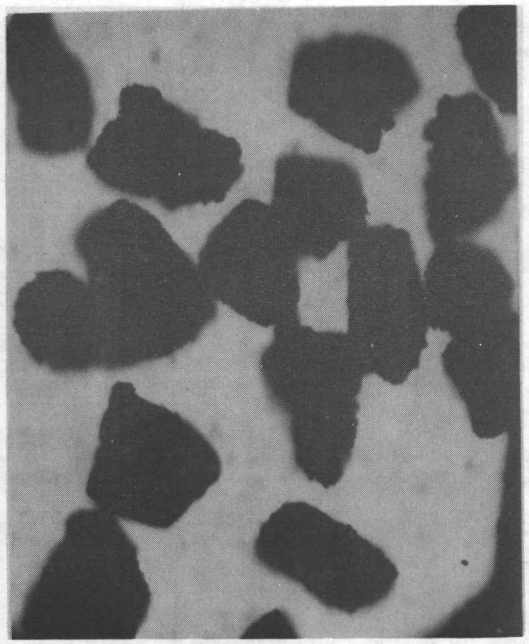

Collector #2

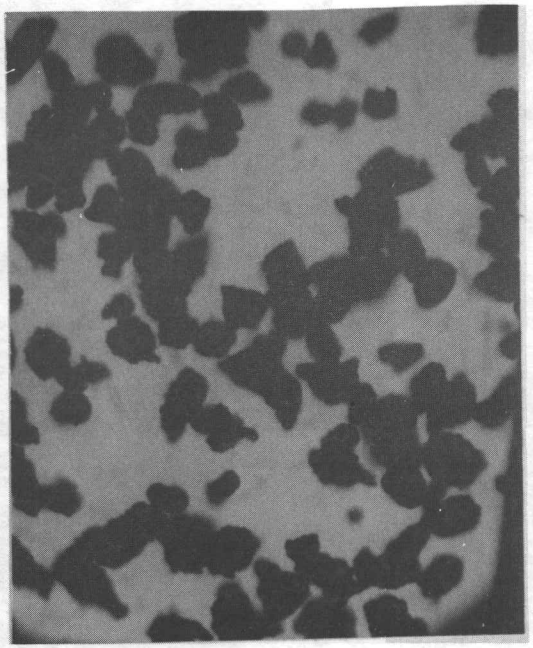

Collector #3

100 μm

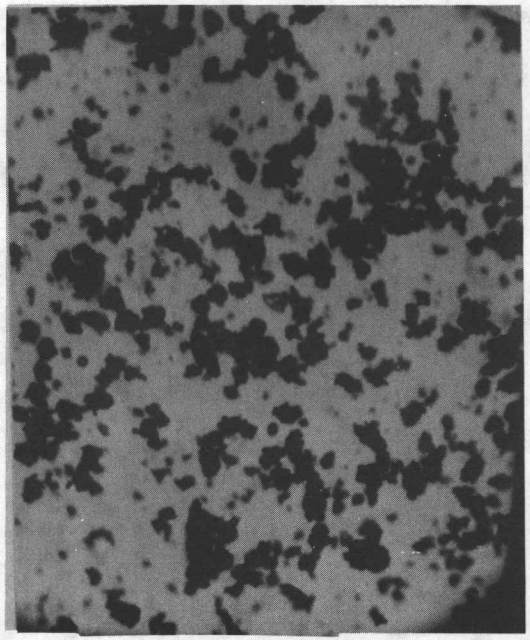

Collector #4

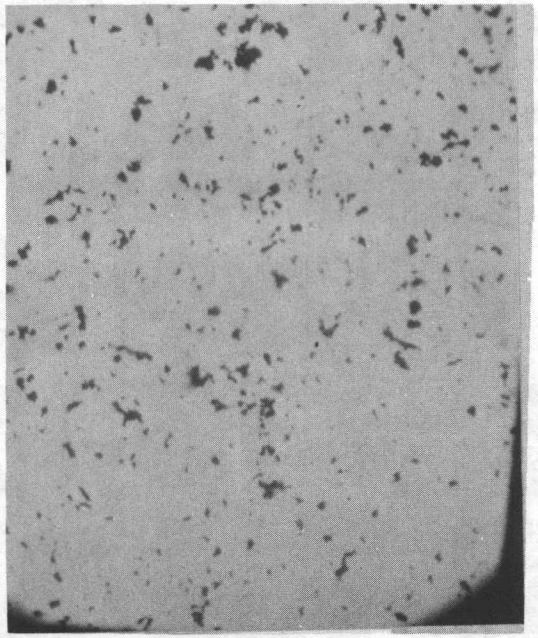

Collector #5

FIG. 23 PHOTOGRAPHS OF SEPARATED CARBON PARTICLES (ALL TO SAME SCALE)

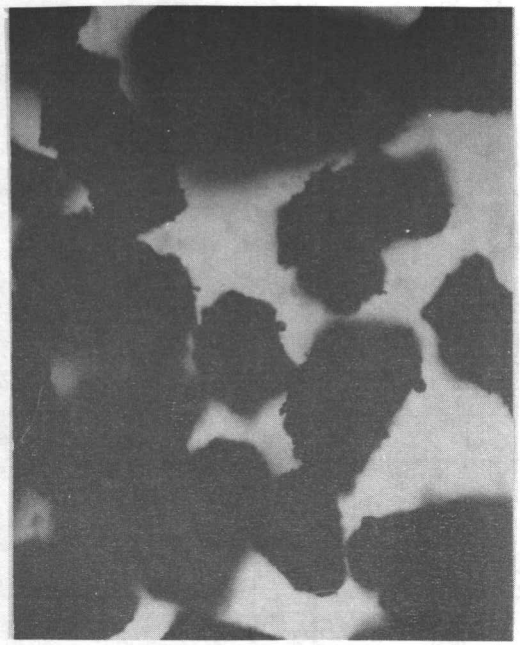

Collector #1

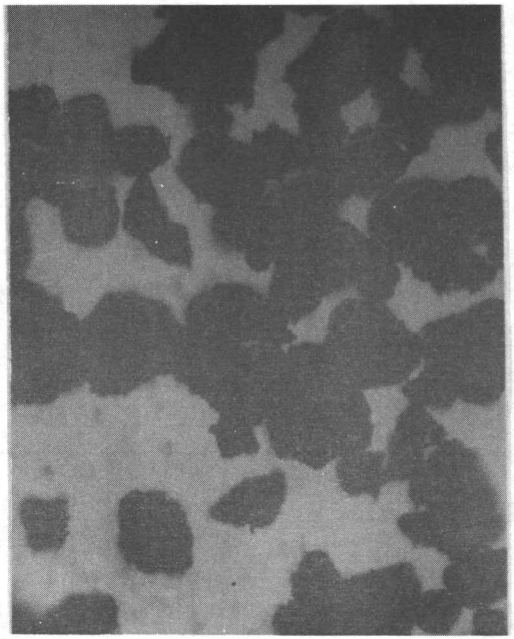

Collector #2

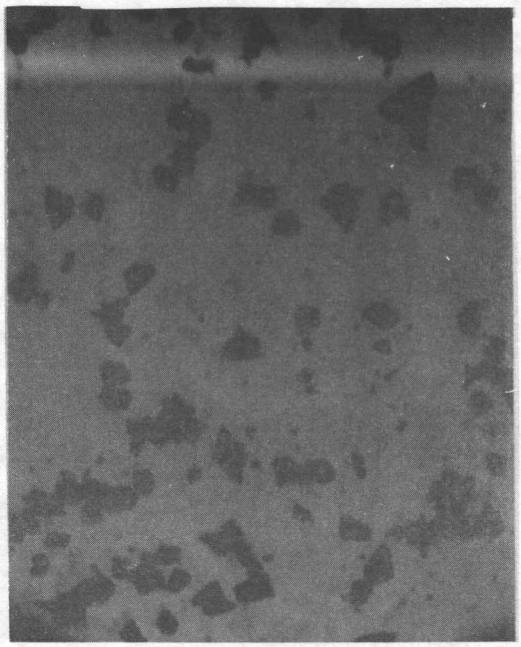

Collector #3

100 μm

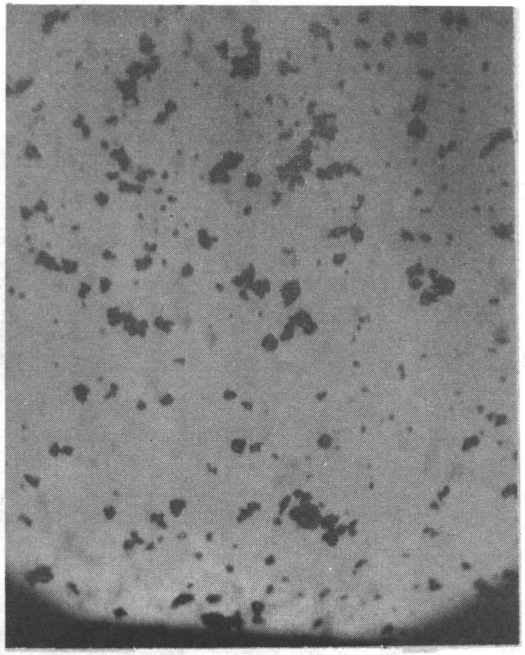

Collector #4

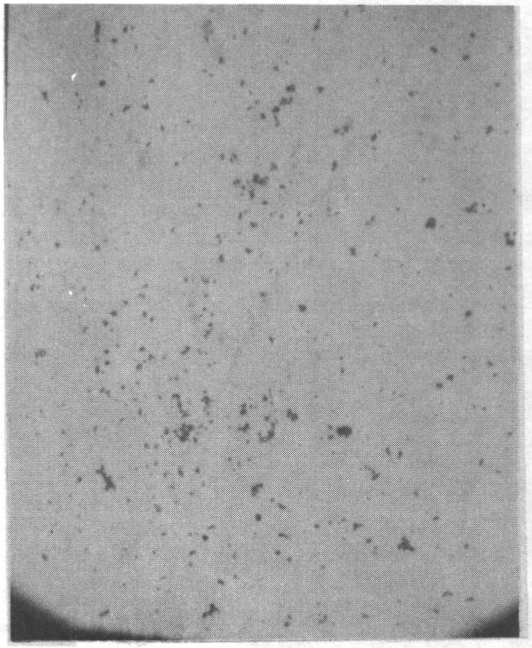

Collector #5

FIG. 24 PHOTOGRAPHS OF SEPARATED CEMENT PARTICLES (ALL TO SAME SCALE)

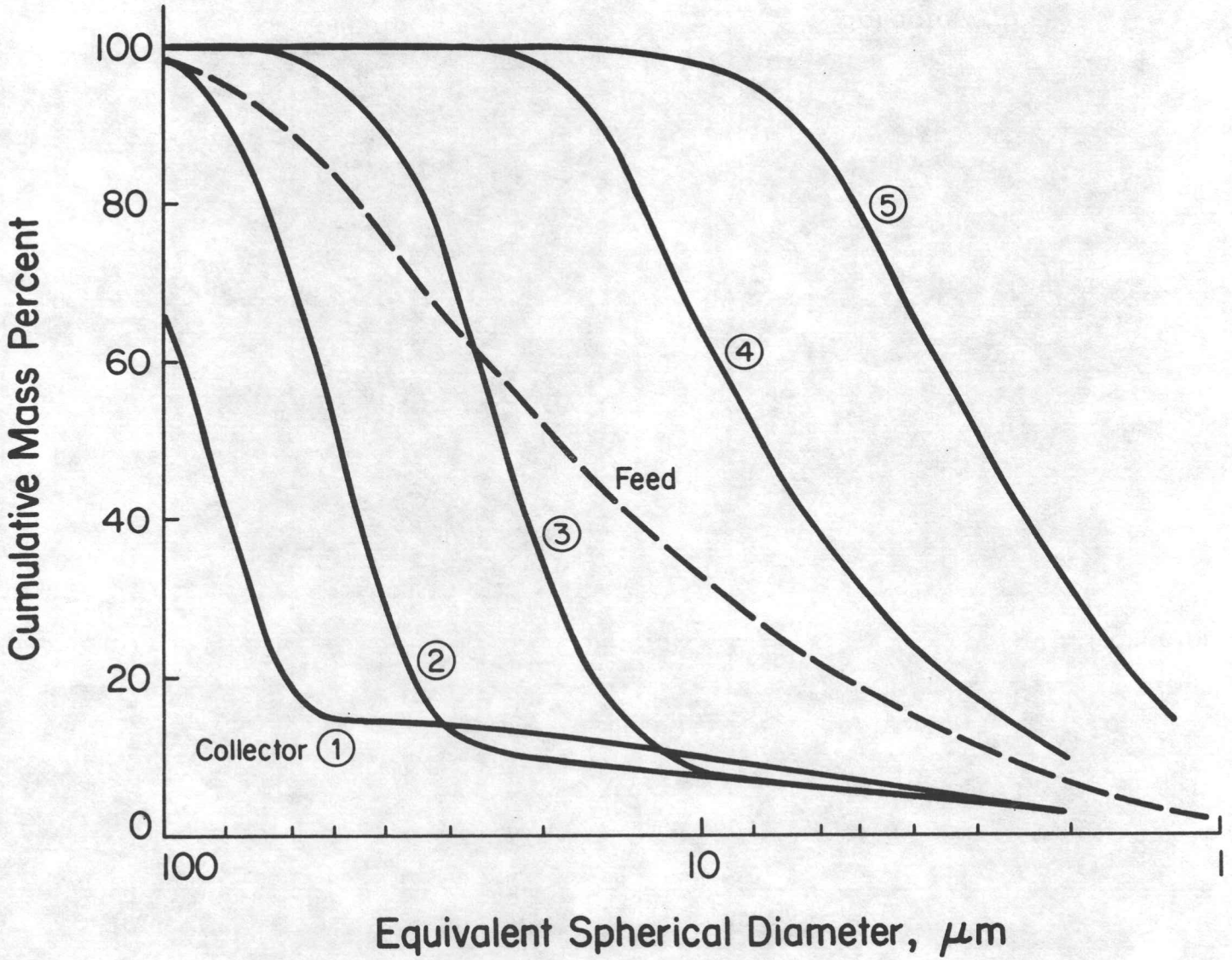

FIG. 25 CUMULATIVE DISTRIBUTIONS FOR A CEMENT SAMPLE

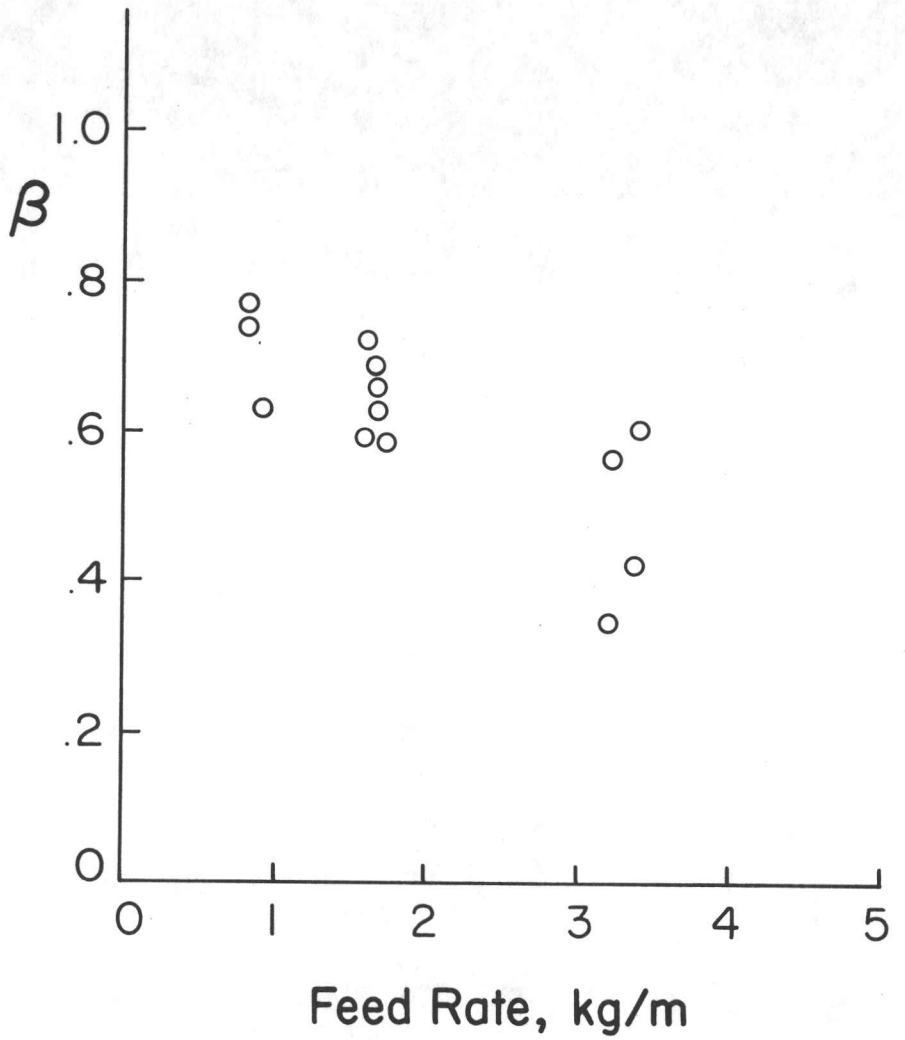

FIG. 26 VARIATION OF SHARPNESS OF CUT WITH FEED RATE FOR CEMENT (SEDIGRAPH DATA), $14 < d_{50} < 47$ μm.

UTIAS Report No. 316

University of Toronto, Institute for Aerospace Studies (UTIAS)
4925 Dufferin Street, Downsview, Ontario, Canada, M3H 5T6

RESEARCH ON AN AERODYNAMIC PARTICLE SEPARATOR (THE EPS)

Etkin, B.

1. Size separation 2. Separators, particle 3. Particle size distribution
4. Particle trajectories 5. Classifiers, air

I. UTIAS Report No. 316 II. Etkin, B.

This report presents an account of the research work carried out in support of the development of a new particle separator. The EPS, as it is designated, produces multiple fractions simultaneously at a high throughput rate. The cut sizes are roughly in the range 10 to 200 μm. The principle is that particles dissimilar with respect to any of size, density, or shape will follow different and distinct trajectories when injected into a uniform laminar flow of air. The main features of the design are:
(1) particles are conveyed pneumatically at high speed into the separation zone;
*(2) they are separated from the feed air at the entrance to the separation zone by means of the Coanda Effect;
(3) the air flow in the separation zone is uniform and laminar, the rms turbulence level being less than 1%; air speed in the separation zone is of the same order as the particle speed;
(4) the particles are subjected to large forces, both aerodynamic and mechanical, at several points on their path from the feed hopper to the separation zone, thus promoting dispersion.
The report contains the theoretical analyses and experimental measurements made to verify the design concepts. A detailed model of the flow field permits the calculation of particle trajectories, and hence the prediction of coarse grade efficiency and sharpness of cut d_{25}/d_{75}. The measurements made with glass spheres and other irregular particles (e.g., carbon, cement) provide a general verification of the analytical results. Sharpness of cut values better than 0.8 are achieved down to cut points of about 10 μm. Maximum throughput rates are not yet known, but separations have been made at 480 kg/hr in a separation zone 100 mm wide. Scale-up to larger capacity is straightforward.

*U.S. Patent allowed and to be issued.

Available copies of this report are limited. Return this card to UTIAS, if you require a copy.

UTIAS Report No. 316
University of Toronto, Institute for Aerospace Studies (UTIAS)
4925 Dufferin Street, Downsview, Ontario, Canada, M3H 5T6
RESEARCH ON AN AERODYNAMIC PARTICLE SEPARATOR (THE EPS)
Etkin, B.
1. Size separation 2. Separators, particle 3. Particle size distribution
4. Particle trajectories 5. Classifiers, air
I. UTIAS Report No. 316 II. Etkin, B.
This report presents an account of the research work carried out in support of the development of a new particle separator. The EPS, as it is designated, produces multiple fractions simultaneously at a high throughput rate. The cut sizes are roughly in the range 10 to 200 μm. The principle is that particles dissimilar with respect to any of size, density, or shape will follow different and distinct trajectories when injected into a uniform laminar flow of air. The main features of the design are:
(1) particles are conveyed pneumatically at high speed into the separation zone;
*(2) they are separated from the feed air at the entrance to the separation zone by means of the Coanda Effect;
(3) the air flow in the separation zone is uniform and laminar, the rms turbulence level being less than 1%; air speed in the separation zone is of the same order as the particle speed;
(4) the particles are subjected to large forces, both aerodynamic and mechanical, at several points on their path from the feed hopper to the separation zone, thus promoting dispersion.
The report contains the theoretical analyses and experimental measurements made to verify the design concepts. A detailed model of the flow field permits the calculation of particle trajectories, and hence the prediction of coarse grade efficiency and sharpness of cut d_{25}/d_{75}. The measurements made with glass spheres and other irregular particles (e.g., carbon, cement) provide a general verification of the analytical results. Sharpness of cut values better than 0.8 are achieved down to cut points of about 10 μm. Maximum throughput rates are not yet known, but separations have been made at 480 kg/hr in a separation zone 100 mm wide. Scale-up to larger capacity is straightforward.
*U.S. Patent allowed and to be issued.
Available copies of this report are limited. Return this card to UTIAS, if you require a copy.

UTIAS Report No. 316
University of Toronto, Institute for Aerospace Studies (UTIAS)
4925 Dufferin Street, Downsview, Ontario, Canada, M3H 5T6
RESEARCH ON AN AERODYNAMIC PARTICLE SEPARATOR (THE EPS)
Etkin, B.
1. Size separation 2. Separators, particle 3. Particle size distribution
4. Particle trajectories 5. Classifiers, air
I. UTIAS Report No. 316 II. Etkin, B.
This report presents an account of the research work carried out in support of the development of a new particle separator. The EPS, as it is designated, produces multiple fractions simultaneously at a high throughput rate. The cut sizes are roughly in the range 10 to 200 μm. The principle is that particles dissimilar with respect to any of size, density, or shape will follow different and distinct trajectories when injected into a uniform laminar flow of air. The main features of the design are:
(1) particles are conveyed pneumatically at high speed into the separation zone;
*(2) they are separated from the feed air at the entrance to the separation zone by means of the Coanda Effect;
(3) the air flow in the separation zone is uniform and laminar, the rms turbulence level being less than 1%; air speed in the separation zone is of the same order as the particle speed;
(4) the particles are subjected to large forces, both aerodynamic and mechanical, at several points on their path from the feed hopper to the separation zone, thus promoting dispersion.
The report contains the theoretical analyses and experimental measurements made to verify the design concepts. A detailed model of the flow field permits the calculation of particle trajectories, and hence the prediction of coarse grade efficiency and sharpness of cut d_{25}/d_{75}. The measurements made with glass spheres and other irregular particles (e.g., carbon, cement) provide a general verification of the analytical results. Sharpness of cut values better than 0.8 are achieved down to cut points of about 10 μm. Maximum throughput rates are not yet known, but separations have been made at 480 kg/hr in a separation zone 100 mm wide. Scale-up to larger capacity is straightforward.
*U.S. Patent allowed and to be issued.
Available copies of this report are limited. Return this card to UTIAS, if you require a copy.

UTIAS Report No. 316
University of Toronto, Institute for Aerospace Studies (UTIAS)
4925 Dufferin Street, Downsview, Ontario, Canada, M3H 5T6
RESEARCH ON AN AERODYNAMIC PARTICLE SEPARATOR (THE EPS)
Etkin, B.
1. Size separation 2. Separators, particle 3. Particle size distribution
4. Particle trajectories 5. Classifiers, air
I. UTIAS Report No. 316 II. Etkin, B.
This report presents an account of the research work carried out in support of the development of a new particle separator. The EPS, as it is designated, produces multiple fractions simultaneously at a high throughput rate. The cut sizes are roughly in the range 10 to 200 μm. The principle is that particles dissimilar with respect to any of size, density, or shape will follow different and distinct trajectories when injected into a uniform laminar flow of air. The main features of the design are:
(1) particles are conveyed pneumatically at high speed into the separation zone;
*(2) they are separated from the feed air at the entrance to the separation zone by means of the Coanda Effect;
(3) the air flow in the separation zone is uniform and laminar, the rms turbulence level being less than 1%; air speed in the separation zone is of the same order as the particle speed;
(4) the particles are subjected to large forces, both aerodynamic and mechanical, at several points on their path from the feed hopper to the separation zone, thus promoting dispersion.
The report contains the theoretical analyses and experimental measurements made to verify the design concepts. A detailed model of the flow field permits the calculation of particle trajectories, and hence the prediction of coarse grade efficiency and sharpness of cut d_{25}/d_{75}. The measurements made with glass spheres and other irregular particles (e.g., carbon, cement) provide a general verification of the analytical results. Sharpness of cut values better than 0.8 are achieved down to cut points of about 10 μm. Maximum throughput rates are not yet known, but separations have been made at 480 kg/hr in a separation zone 100 mm wide. Scale-up to larger capacity is straightforward.
*U.S. Patent allowed and to be issued.
Available copies of this report are limited. Return this card to UTIAS, if you require a copy.